

Next-to-leading order QCD predictions for associated production of top squarks and charginos at the CERN LHC

Li Gang Jin, Chong Sheng Li*, and Jian Jun Liu

Department of Physics, Peking University, Beijing 100871, P.R. China

Abstract

We present the calculations of the complete next-to-leading order (NLO) inclusive total cross sections for the associated production processes $pp \rightarrow \tilde{t}_i \tilde{\chi}_k^- + X$ in the Minimal Supersymmetric Standard Model at the CERN Large Hadron Collider. Our calculations show that the total cross sections for the $\tilde{t}_1 \tilde{\chi}_1^-$ production for the lighter top squark masses in the region $100 \text{ GeV} < m_{\tilde{t}_1} < 160 \text{ GeV}$ can reach 1 pb in the favorable parameter space allowed by the current precise experiments, and in other cases the total cross sections generally vary from 10 fb to several hundred fb except both $m_{\tilde{t}_1} > 500 \text{ GeV}$ and the $\tilde{t}_2 \tilde{\chi}_2^-$ production channel. Moreover, we find that the NLO QCD corrections in general enhance the leading order total cross sections significantly, and vastly reduce the dependence of the total cross sections on the renormalization/factorization scale, which leads to increased confidence in predictions based on these results.

PACS numbers: 12.60.Jv, 12.38.Bx, 13.85.Fb

* E-mail: csli@pku.edu.cn

I. INTRODUCTION

The CERN Large Hadron Collider (LHC), with $\sqrt{S} = 14$ TeV and a luminosity of 100 fb^{-1} per year [1], will be a wonderful machine for discovering new physics. In so many new physical models, the Minimal Supersymmetric Standard Model (MSSM) [2] is one of the most attractive models for the theorists and the high energy experimenters, and searching for supersymmetric (SUSY) particles, as a direct experimental evidence, is one of the prime objectives at the LHC. Therefore, a good understanding of theoretical predictions of the cross sections for the production of the SUSY particles is important.

The cross sections for the production of squarks and gluinos were calculated at the Born level already many years ago [3]. To date, the productions of gluinos and squarks [4, 5], top squarks [6], sleptons [7, 8] and gauginos [7] at the hadron colliders have been studied. Besides the leading order (LO) results, these calculations also have included the next-to-leading order (NLO) corrections to improve the accuracy of the theoretical predictions and reduce the uncertainty from the dependence of results on renormalization/factorization scale. It was recently pointed out in Ref. [9] that the associated production of a gluino (\tilde{g}) with a gaugino ($\tilde{\chi}$) or with a squark (\tilde{q}) is potentially a very important production mechanism, since the mass spectrum favors much lighter masses for the color-neutral charginos and neutralinos than for the colored squarks and gluinos in popular models of SUSY breaking. And a detailed NLO QCD calculation of the associated production of a gluino and a gaugino at the Tevatron and the LHC has been given in Ref. [9]. However, the processes of the associated gaugino and squark productions have not been calculated at LO and NLO yet.

In this paper, we present the complete NLO QCD (including SUSY QCD) calculation for the cross sections of the associated production of top squarks (stops) and charginos at the LHC. Similar to $pp \rightarrow gb \rightarrow tH^-$ [10], which is expected to be a dominate process for the charged Higgs boson production at the LHC, the associated production $pp \rightarrow gb \rightarrow \tilde{t}_i \tilde{\chi}_k^-$ may be also the dominate process for single top squark or chargino production at the LHC. This is due to the following reasons: first, the large top quark mass in stop mass matrix can lead to strong mixing, and induce large mass difference between the lighter mass eigenstate and the heavier one, which means that the phase space for the lighter stop will be great and benefit its production; second, besides containing a strong QCD coupling between the incoming partons, this process also includes an enhanced effects from the Yukawa coupling

in the vertex $b-\tilde{t}_i-\tilde{\chi}_k^-$ of the final states. For simplicity, in this paper we neglect the bottom quark mass except in the Yukawa coupling. Such approximations are valid in all diagrams, in which the bottom quark appears as an initial state parton, according to the simplified Aivazis-Collins-Olness-Tung (ACOT) scheme [11]. However, it was pointed out in Ref. [12] that the approximations of the hard process kinematics and the introduction of conventional bottom quark densities will give rise to sizable bottom quark mass and kinematical phase space effects, and may overestimate the inclusive cross section, for example, in the processes of $b\bar{b} \rightarrow H$ [13] and $bg \rightarrow bH$ [14]. Very recently, it is shown in Ref. [15] that the bottom parton approach is still valid if we choose the factorization scale below the average final state mass: $\mu_f \sim Cm_{\text{av}} \equiv C(m_{\tilde{t}_i} + m_{\tilde{\chi}_k^-})/2$ with $C \sim (1/4, \dots, 1/3)$. Thus, in this paper, we choose $\mu_f = m_{\text{av}}/3$ when we use the bottom parton approximation.

The arrangement of this paper is as follows. In Sec. II we show the LO results and define the notations. In Sec. III we present the details of the calculations of both the virtual and real parts of the NLO QCD corrections. In Sec. IV by a detailed numerical analysis we present the predictions for inclusive and differential cross sections at the LHC. The lengthy analytic expressions are summarized in Appendixes A and B.

II. LEADING ORDER PRODUCTION OF STOPS AND CHARGINOS

The partonic process of the LO associated production of stops and charginos is $g(p_a)b(p_b) \rightarrow \tilde{t}_i(p_1)\tilde{\chi}_k^-(p_2)$, and the related Feynman diagrams are shown in Fig. 1. In order to simplify our expressions, we introduce the following Mandelstam variables:

$$\begin{aligned}
s &= (p_a + p_b)^2, & s_\Delta &= s - m_{\tilde{t}_i}^2 - m_{\tilde{\chi}_k^-}^2, \\
t &= (p_a - p_1)^2, & t_1 &= t - m_{\tilde{t}_i}^2, & t_2 &= t - m_{\tilde{\chi}_k^-}^2, \\
u &= (p_a - p_2)^2, & u_1 &= u - m_{\tilde{t}_i}^2, & u_2 &= u - m_{\tilde{\chi}_k^-}^2.
\end{aligned} \tag{2.1}$$

After the n -dimensional phase space integration, the LO partonic differential cross sections are given by ($n = 4 - 2\epsilon$)

$$\begin{aligned}
\frac{d^2\hat{\sigma}_{ik}^B}{dt_2du_2} &= \frac{\pi S_\epsilon}{s^2\Gamma(1-\epsilon)} \left(\frac{t_2u_2 - sm_{\tilde{\chi}_k^-}^2}{\mu_r^2s} \right)^{-\epsilon} \Theta(t_2u_2 - sm_{\tilde{\chi}_k^-}^2) \Theta[s - (m_{\tilde{t}_i} + m_{\tilde{\chi}_k^-})^2] \\
&\quad \times \delta(s + t + u - m_{\tilde{t}_i}^2 - m_{\tilde{\chi}_k^-}^2) |\overline{M_{ik}^B}|^2
\end{aligned} \tag{2.2}$$

with

$$\overline{|M_{ik}^B|^2} = \frac{g^2 g_s^2}{12(1-\epsilon)} (|l_{ik}^{\tilde{t}}|^2 + |k_{ik}^{\tilde{t}}|^2) \left(-\frac{t_2 + (1-\epsilon)u_2}{s} + \frac{ss_\Delta - u_1(u_2 + 2t_2)}{st_1} + \frac{2t_2 m_{\tilde{t}_i}^2}{t_1^2} \right), \quad (2.3)$$

where $S_\epsilon = (4\pi)^{-2+\epsilon}$, and the indices (i, k) label the outgoing particles $(\tilde{t}_i, \tilde{\chi}_k^-)$. The scale parameter μ_r is introduced to provide the correct mass dimension for the coupling constant in n -dimensions. $\overline{|M_{ik}^B|^2}$ is the LO squared matrix element, which has been summed the colors and spins of the outgoing particles, and averaged over the colors and spins of the incoming ones. $l_{ik}^{\tilde{t}}$ and $k_{ik}^{\tilde{t}}$ are the left- and right- handed coupling constants of the vertex $b - \tilde{t}_i - \tilde{\chi}_k^-$, respectively, and are defined together with $l_{ik}^{\tilde{b}}$ and $k_{ik}^{\tilde{b}}$ in the vertex $t - \tilde{b}_i - \tilde{\chi}_k^+$, which is involved in the virtual corrections, as follows:

$$\begin{pmatrix} l_{ik}^{\tilde{t}} \\ l_{ik}^{\tilde{b}} \end{pmatrix} = - \begin{pmatrix} R_{i1}^{\tilde{t}} V_{k1}^* \\ R_{i1}^{\tilde{b}} U_{k1}^* \end{pmatrix} + \begin{pmatrix} Y_t R_{i2}^{\tilde{t}} V_{k2}^* \\ Y_b R_{i2}^{\tilde{b}} U_{k2}^* \end{pmatrix}, \quad \begin{pmatrix} k_{ik}^{\tilde{t}} \\ k_{ik}^{\tilde{b}} \end{pmatrix} = \begin{pmatrix} Y_b R_{i1}^{\tilde{t}} U_{k2} \\ Y_t R_{i1}^{\tilde{b}} V_{k2} \end{pmatrix} \quad (2.4)$$

with

$$Y_t \equiv \frac{m_t}{\sqrt{2}m_W \sin \beta} \equiv \frac{h_t}{g}, \quad Y_b \equiv \frac{m_b}{\sqrt{2}m_W \cos \beta} \equiv \frac{h_b}{g}. \quad (2.5)$$

Here the angle β is defined by $\tan \beta \equiv v_2/v_1$, the ratio of the vacuum expectation values of the two Higgs doublets. Matrices U and V are the chargino transformation matrices from interaction to mass eigenstates defined in Ref. [16]. Matrix $R^{\tilde{q}}$ ($q = t, b$) is defined to transform the current eigenstates \tilde{q}_L and \tilde{q}_R to the mass eigenstates \tilde{q}_1 and \tilde{q}_2 :

$$\begin{pmatrix} \tilde{q}_1 \\ \tilde{q}_2 \end{pmatrix} = R^{\tilde{q}} \begin{pmatrix} \tilde{q}_L \\ \tilde{q}_R \end{pmatrix}, \quad R^{\tilde{q}} = \begin{pmatrix} \cos \theta_{\tilde{q}} & \sin \theta_{\tilde{q}} \\ -\sin \theta_{\tilde{q}} & \cos \theta_{\tilde{q}} \end{pmatrix} \quad (2.6)$$

with $0 \leq \theta_{\tilde{q}} < \pi$ by convention. Correspondingly, the mass eigenvalues $m_{\tilde{q}_1}$ and $m_{\tilde{q}_2}$ (with $m_{\tilde{q}_1} \leq m_{\tilde{q}_2}$) are given by

$$\begin{pmatrix} m_{\tilde{q}_1}^2 & 0 \\ 0 & m_{\tilde{q}_2}^2 \end{pmatrix} = R^{\tilde{q}} M_{\tilde{q}}^2 (R^{\tilde{q}})^\dagger, \quad M_{\tilde{q}}^2 = \begin{pmatrix} m_{\tilde{q}_L}^2 & a_q m_q \\ a_q m_q & m_{\tilde{q}_R}^2 \end{pmatrix} \quad (2.7)$$

with

$$m_{\tilde{q}_L}^2 = M_{\tilde{Q}}^2 + m_q^2 + m_Z^2 \cos 2\beta (I_{3L}^q - e_q \sin^2 \theta_W), \quad (2.8)$$

$$m_{\tilde{q}_R}^2 = M_{\{\tilde{U}, \tilde{D}\}}^2 + m_q^2 + m_Z^2 \cos 2\beta e_q \sin^2 \theta_W, \quad (2.9)$$

$$a_q = A_q - \mu \{ \cot \beta, \tan \beta \} \quad (2.10)$$

for {up, down} type squarks. Here $M_{\tilde{q}}^2$ is the squark mass matrix. $M_{\tilde{Q},\tilde{U},\tilde{D}}$ and $A_{t,b}$ are soft SUSY-breaking parameters and μ is the Higgs mixing parameter in the superpotential. I_{3L}^q and e_q are the third component of the weak isospin and the electric charge of the quark q , respectively.

The LO total cross section at the LHC is obtained by convoluting the partonic cross section with the parton distribution functions (PDFs) $G_{b,g/p}$ in the proton:

$$\sigma_{ik}^B = \int dx_1 dx_2 [G_{b/p}(x_1, \mu_f) G_{g/p}(x_2, \mu_f) + (x_1 \leftrightarrow x_2)] \hat{\sigma}_{ik}^B, \quad (2.11)$$

where μ_f is the factorization scale.

III. NEXT-TO-LEADING ORDER CALCULATIONS

The NLO contributions to the associated production of stops and charginos can be separated into the virtual corrections arising from loop diagrams of colored particles and the real corrections arising from the radiations of a real gluon or a massless (anti)quark.

A. Virtual Corrections

The virtual corrections to $gb \rightarrow \tilde{t}_i \tilde{\chi}_k^-$ arise from the Feynman diagrams shown in Fig. 2 and 3, which consist of self-energy, vertex and box diagrams. We carried out the calculation in t'Hooft-Feynman gauge and used the dimensional regularization in $n = 4 - 2\epsilon$ dimensions to regularize the ultraviolet (UV), soft infrared and collinear divergences in the virtual loop corrections. However, this method violates the supersymmetry. In order to restore the supersymmetry the simplest procedure is through finite shifts in the quark-squark-gluino(chargino) couplings [17]:

$$\begin{aligned} \hat{g}_s &= g_s \left[1 + \frac{\alpha_s}{8\pi} \left(\frac{4}{3} N - C_F \right) \right], \\ \hat{e} &= e \left(1 - \frac{\alpha_s}{8\pi} C_F \right), \\ \hat{h}_{t,b} &= h_{t,b} \left(1 - \frac{3\alpha_s}{8\pi} C_F \right) \end{aligned} \quad (3.1)$$

with $N = 3$ and $C_F = 4/3$. Since we have not such a coupling as $\tilde{g} - q - \tilde{q}$ at the tree-level, the first shift is not used in our calculations, and we just consider the latter two shifts. As for the Dirac matrix γ_5 , we deal with it using the ‘naive’ scheme, in which the γ_5 -matrix

anticommutes with the other γ_μ -matrices. This is a legitimate procedure at the one-loop level for anomaly-free theories [18].

The virtual corrections to the differential cross section can be expressed as

$$\begin{aligned} \frac{d^2 \hat{\sigma}_{ik}^V}{dt_2 du_2} &= \frac{\pi S_\epsilon}{s^2 \Gamma(1-\epsilon)} \left(\frac{t_2 u_2 - sm_{\tilde{\chi}_k^-}^2}{\mu_r^2 s} \right)^{-\epsilon} \Theta(t_2 u_2 - sm_{\tilde{\chi}_k^-}^2) \Theta[s - (m_{\tilde{t}_i} + m_{\tilde{\chi}_k^-})^2] \\ &\quad \times \delta(s + t + u - m_{\tilde{t}_i}^2 - m_{\tilde{\chi}_k^-}^2) 2 \operatorname{Re}(\overline{M_{ik}^V} M_{ik}^{B*}), \end{aligned} \quad (3.2)$$

where M_{ik}^V is the renormalized amplitude, which can be separated into two parts:

$$M_{ik}^V = M_{ik}^{unren} + M_{ik}^{con}. \quad (3.3)$$

Here M_{ik}^{unren} contains the self-energy, vertex and box corrections, and M_{ik}^{con} is the corresponding counterterm. Moreover, M_{ik}^{unren} can be written as

$$M_{unren} = \sum_{\alpha=a}^f M_{ik}^\alpha + \sum_{\beta=a}^g M_{ik}^{box(\beta)}, \quad (3.4)$$

where α and β denote the corresponding diagram indexes in Fig. 2 and Fig. 3, respectively.

We express each term further as

$$M_{ik}^\alpha = C_s \sum_{l=1}^{12} f_l^\alpha M_l, \quad (3.5)$$

$$M_{ik}^{box(\beta)} = C_s \sum_{l=1}^{12} f_l^{box(\beta)} M_l, \quad (3.6)$$

where $C_s = igg_s^3/(16\pi^2)$, f_l^α and $f_l^{box(\beta)}$ are the form factors, which are given explicitly in Appendix A, and M_l are the standard matrix elements defined as

$$\begin{aligned} M_{1,2} &= v^T(p_2) C^{-1} T^a \not{\epsilon}(p_a) P_{L,R} u(p_b), \\ M_{3,4} &= v^T(p_2) C^{-1} T^a \not{p}_a \not{\epsilon}(p_a) P_{L,R} u(p_b), \\ M_{5,6} &= v^T(p_2) C^{-1} T^a P_{L,R} u(p_b) p_b \cdot \epsilon(p_a), \\ M_{7,8} &= v^T(p_2) C^{-1} T^a P_{L,R} u(p_b) p_2 \cdot \epsilon(p_a), \\ M_{9,10} &= v^T(p_2) C^{-1} T^a \not{p}_a P_{L,R} u(p_b) p_b \cdot \epsilon(p_a), \\ M_{11,12} &= v^T(p_2) C^{-1} T^a \not{p}_a P_{L,R} u(p_b) p_2 \cdot \epsilon(p_a). \end{aligned} \quad (3.7)$$

Here C is the charge conjugation operator, and T^a is the $SU(3)$ color matrix.

M_{ik}^{con} is separated into $M_{ik}^{con(s)}$ and $M_{ik}^{con(t)}$, i.e. the counterterms for s and t channels, respectively, which are given by ($j \neq i$)

$$\begin{aligned}
M_{ik}^{con} &= M_{ik}^{con(s)} + M_{ik}^{con(t)}, \\
M_{ik}^{con(s)} &= -\frac{ig_g s}{s} \{ [l_{ik}^{\bar{t}} \Delta + l_{jk}^{\bar{t}} \delta Z_{ji}^{\bar{t}} + \delta l_{ik}^{\bar{t}}] (M_3 + 2M_5) + [k_{ik}^{\bar{t}} \Delta + k_{jk}^{\bar{t}} \delta Z_{ji}^{\bar{t}} + \delta k_{ik}^{\bar{t}}] (M_4 + 2M_6) \}, \\
M_{ik}^{con(t)} &= -i2gg_s \{ [\frac{l_{ik}^{\bar{t}}}{t_1} (\Delta + \frac{\delta m_{\bar{t}_i}^2}{t_1}) + \frac{\delta l_{ik}^{\bar{t}}}{t_1} + \frac{l_{jk}^{\bar{t}} \delta Z_{ji}^{\bar{t}}}{t - m_{\bar{t}_j}^2}] (M_5 - M_7) + [\frac{k_{ik}^{\bar{t}}}{t_1} (\Delta + \frac{\delta m_{\bar{t}_i}^2}{t_1}) \\
&\quad + \frac{\delta k_{ik}^{\bar{t}}}{t_1} + \frac{k_{jk}^{\bar{t}} \delta Z_{ji}^{\bar{t}}}{t - m_{\bar{t}_j}^2}] (M_6 - M_8) \},
\end{aligned}$$

with

$$\begin{aligned}
\Delta &= \frac{\delta g_s}{g_s} + \frac{1}{2} \delta Z_g + \frac{1}{2} \delta Z_b + \frac{1}{2} \delta Z_{ii}^{\bar{t}}, \\
\delta l_{ik}^{\bar{t}} &= R_{i2}^{\bar{t}} V_{k1}^* \delta \theta^{\bar{t}} + Y_t V_{k2}^* (R_{i2}^{\bar{t}} \frac{\delta m_t}{m_t} + R_{i1}^{\bar{t}} \delta \theta^{\bar{t}}), \\
\delta k_{ik}^{\bar{t}} &= Y_b U_{k2} (R_{i1}^{\bar{t}} \frac{\delta m_b}{m_b} - R_{i2}^{\bar{t}} \delta \theta^{\bar{t}}).
\end{aligned}$$

where $\delta m_{\bar{t}_i}^2$, δm_q ($q = t, b$), δZ_b , δZ_g , $\delta Z_{ii}^{\bar{t}}$, $\delta Z_{ij}^{\bar{t}}$ and $\delta \theta_{\bar{t}}$ are the renormalization constants, which are fixed by the on-shell renormalization scheme [19], and can be written as (assuming $m_{\bar{b}_1} = m_{\bar{b}_2}$)

$$\begin{aligned}
\delta m_{\bar{t}_i}^2 &= -\frac{\alpha_s}{4\pi} C_F \{ 4m_{\bar{t}_i}^2 B_0(m_{\bar{t}_i}^2, m_{\bar{t}_i}^2, 0) - A_0(m_{\bar{t}_i}^2) + 4A_0(m_t^2) + 4[m_{\bar{t}_i}^2 B_1 + m_{\bar{g}}^2 B_0 \\
&\quad - 2m_t m_{\bar{g}} R_{i1}^{\bar{t}} R_{i2}^{\bar{t}} B_0](m_{\bar{t}_i}^2, m_{\bar{g}}^2, m_t^2) \}, \\
\frac{\delta m_q}{m_q} &= -\frac{\alpha_s}{4\pi} C_F \{ (4B_0 + 2B_1)(m_q^2, m_q^2, 0) - 1 + \sum_{i=1}^2 [B_1 - \frac{m_{\bar{g}}}{m_q} \sin 2\theta_{\bar{q}} (-1)^i B_0](m_q^2, m_{\bar{g}}^2, m_{\bar{q}_i}^2) \}, \\
\delta Z_b &= \frac{\alpha_s}{2\pi} C_F B_1(0, m_{\bar{g}}^2, m_{\bar{b}_1}^2), \\
\delta Z_g &= -\frac{\alpha_s}{4\pi} [\frac{2}{3} (B_0 + 2m_t^2 B_0')(0, m_t^2, m_t^2) + 2(B_0 + 2m_{\bar{g}}^2 B_0')(0, m_{\bar{g}}^2, m_{\bar{g}}^2) \\
&\quad + \frac{2}{3} \sum_{q,i} (\frac{1}{4} B_0 - m_{\bar{q}_i}^2 B_0')(0, m_{\bar{q}_i}^2, m_{\bar{q}_i}^2) - \frac{7}{9}], \\
\delta Z_{ii}^{\bar{t}} &= \frac{\alpha_s}{2\pi} C_F \{ (B_0 + 2m_{\bar{t}_i}^2 B_0')(m_{\bar{t}_i}^2, m_{\bar{t}_i}^2, 0) - [B_0 + (m_{\bar{t}_i}^2 - m_{\bar{g}}^2 - m_t^2) B_0' \\
&\quad + 4m_t m_{\bar{g}} R_{i1}^{\bar{t}} R_{i2}^{\bar{t}} B_0'](m_{\bar{t}_i}^2, m_{\bar{g}}^2, m_t^2) \}, \\
\delta Z_{ij}^{\bar{t}} &= \frac{\text{Re} \Sigma_{ij}^{\bar{t}}(m_{\bar{t}_j}^2)}{m_{\bar{t}_i}^2 - m_{\bar{t}_j}^2}, \\
\delta \theta_{\bar{t}} &= \frac{\text{Re} [\Sigma_{12}^{\bar{t}}(m_{\bar{t}_1}^2) + \Sigma_{12}^{\bar{t}}(m_{\bar{t}_2}^2)]}{2(m_{\bar{t}_1}^2 - m_{\bar{t}_2}^2)},
\end{aligned}$$

where $B'_0 = \partial B_0 / \partial p^2$, A_0 and B_i are the Passarino-Veltman one-point and two-point integrals, respectively, which are defined similar to Ref. [20] except that we take internal masses squared as arguments. Here the counterterm $\delta\theta_{\bar{t}}$ for the stop mixing angle is fixed as Ref. [21], and

$$\Sigma_{ij}^{\bar{t}} = \frac{\alpha_s}{4\pi} \frac{2}{3} \{ \sin 4\theta_{\bar{t}} [A_0(m_{\bar{t}_2}^2) - A_0(m_{\bar{t}_1}^2)] + 8m_{\bar{t}} m_{\bar{g}} \cos 2\theta_{\bar{t}} B_0(m_{\bar{t}_j}^2, m_{\bar{g}}^2, m_{\bar{t}}^2) \}.$$

In $\delta Z_{ii}^{\bar{t}}$, $B'_0(m_{\bar{t}_i}^2, m_{\bar{t}_i}^2, 0)$ contains infrared divergences, and can be expressed as

$$B'_0(m_{\bar{t}_i}^2, m_{\bar{t}_i}^2, 0) = -\frac{1}{2m_{\bar{t}_i}^2} \left(\frac{4\pi\mu_r^2}{m_{\bar{t}_i}^2} \right)^\epsilon \Gamma(1+\epsilon) \left(\frac{1}{\epsilon} + 2 \right).$$

Moreover, the QCD coupling constant g_s is renormalized in the modified minimal subtraction (\overline{MS}) scheme except that the divergences associated with the top quark and colored SUSY particle loops are subtracted at zero momentum [22]. Assuming that the scalar partners of the $n_f = 5$ light quark flavors have a common mass $m_{\bar{q}}$, we obtain

$$\frac{\delta g_s}{g_s} = -\frac{\alpha_s(\mu_r^2)}{4\pi} \left[\frac{\beta_0}{2} \frac{1}{\bar{\epsilon}} + \frac{N}{3} \ln \frac{m_{\bar{g}}^2}{\mu_r^2} + \frac{n_f}{6} \ln \frac{m_{\bar{q}}^2}{\mu_r^2} + \frac{1}{12} \ln \frac{m_{\bar{t}_1}^2}{\mu_r^2} + \frac{1}{12} \ln \frac{m_{\bar{t}_2}^2}{\mu_r^2} + \frac{1}{3} \ln \frac{m_{\bar{t}}^2}{\mu_r^2} \right], \quad (3.8)$$

which agrees with one given in Ref. [4]. Here $1/\bar{\epsilon} = 1/\epsilon_{UV} - \gamma_E + \ln(4\pi)$, and

$$\beta_0 = \left(\frac{11}{3}N - \frac{2}{3}n_f \right) + \left[-\frac{2}{3}(N+1) - \frac{1}{3}(n_f+1) \right] \equiv \beta_0^L + \beta_0^H, \quad (3.9)$$

where β_0^L includes the contributions from the gluon and the quarks except the top quark, and β_0^H contains the contributions from the top quark and all colored SUSY particles. The evolution of g_s is determined by β_0^L . After renormalization, M_{ik}^V is UV-finite, but it still contains the infrared (IR) divergences:

$$M_{ik}^V|_{IR} = \frac{\alpha_s}{2\pi} \Gamma(1+\epsilon) \left(\frac{4\pi\mu_r^2}{s} \right)^\epsilon \left(\frac{A_2^V}{\epsilon^2} + \frac{A_1^V}{\epsilon} \right) M_{ik}^B, \quad (3.10)$$

where

$$A_2^V = -\frac{13}{3}, \quad (3.11)$$

$$A_1^V = -\frac{43}{6} - \frac{4}{3} \ln \frac{s}{m_{\bar{t}_i}^2} + 3 \ln \frac{-t_1}{m_{\bar{t}_i}^2} - \frac{1}{3} \ln \frac{-u_1}{m_{\bar{t}_i}^2}. \quad (3.12)$$

Here the infrared divergences include the soft infrared divergences and the collinear infrared divergences. The soft infrared divergences can be cancelled by adding the real corrections, and the remaining collinear infrared divergences can be absorbed into the redefinition of PDF [23], which will be discussed in the following subsections.

B. Real Gluon Emission

The Feynman diagrams of the real gluon emission process $g(p_a)b(p_b) \rightarrow \tilde{t}_i(p_1)\tilde{\chi}_k^-(p_2) + g(p_3)$ are shown in Fig.4. Using the notations analogous to ones defined in Ref. [24], we express our results in terms of the following invariants:

$$\begin{aligned}
s &= (p_a + p_b)^2, & s_5 &= (p_1 + p_2)^2, & s_{5\Delta} &= s_5 - \Delta_s, \\
s_3 &= (p_2 + p_3)^2 - m_{\tilde{t}_i}^2, & s_4 &= (p_1 + p_3)^2 - m_{\tilde{t}_i}^2, & s_{3\Delta} &= s_3 - \Delta_t, \\
t &= (p_b - p_2)^2, & t' &= (p_b - p_3)^2, & t_1 &= t - m_{\tilde{t}_i}^2, & t_2 &= t - m_{\tilde{\chi}_k^-}^2, \\
u &= (p_a - p_2)^2, & u' &= (p_a - p_3)^2, & u_1 &= u - m_{\tilde{t}_i}^2, & u_2 &= u - m_{\tilde{\chi}_k^-}^2, \\
u_6 &= (p_b - p_1)^2 - m_{\tilde{t}_i}^2, & u_7 &= (p_a - p_1)^2 - m_{\tilde{t}_i}^2, & & & &
\end{aligned} \tag{3.13}$$

where $\Delta_s = m_{\tilde{t}_i}^2 + m_{\tilde{\chi}_k^-}^2$ and $\Delta_t = m_{\tilde{\chi}_k^-}^2 - m_{\tilde{t}_i}^2$.

The phase space integration for the real gluon emission will produce infrared singularities, which can be either soft or collinear and can be conveniently isolated by slicing the phase space into different regions defined by suitable cutoffs. In this paper, we use the two cutoff phase space slicing method [25] to decompose the three-body phase space into three regions.

First, the phase space can be separated into two regions by an arbitrary small soft cutoff δ_s , according to whether the energy of the emitted gluon is soft, i.e. $E_3 \leq \delta_s\sqrt{s}/2$, or hard, i.e. $E_3 > \delta_s\sqrt{s}/2$. Correspondingly, the partonic real cross section can be written as

$$\hat{\sigma}_{ik}^R = \hat{\sigma}_{ik}^S + \hat{\sigma}_{ik}^H, \tag{3.14}$$

where $\hat{\sigma}_{ik}^S$ and $\hat{\sigma}_{ik}^H$ are the contributions from the soft and hard regions, respectively. $\hat{\sigma}_{ik}^S$ contains all the soft infrared divergences, which can be explicitly obtained after the integration over the phase space of the emitted gluon. Second, to isolate the remaining collinear divergences from $\hat{\sigma}_{ik}^H$, we should introduce another arbitrary small cutoff, called collinear cutoff δ_c , to further split the hard gluon phase space into two regions, according to whether the Mandelstam variables satisfy the collinear condition $0 < -t'$ ($-u'$) $< \delta_c s$ or not. Then we have

$$\hat{\sigma}_{ik}^H = \hat{\sigma}_{ik}^{HC} + \hat{\sigma}_{ik}^{\overline{HC}}, \tag{3.15}$$

where the hard collinear part $\hat{\sigma}_{ik}^{HC}$ contains the collinear divergences, which can be explicitly obtained after the integration over the phase space of the emitted gluon. And the hard non-collinear part $\hat{\sigma}_{ik}^{\overline{HC}}$ is finite and can be numerically computed using standard Monte-Carlo

integration techniques [26], and can be written as

$$d\hat{\sigma}_{ik}^{\overline{HC}} = \frac{1}{2s} \overline{|M_{ik}^{gb}|^2} d\overline{\Gamma}_3. \quad (3.16)$$

Here $d\overline{\Gamma}_3$ is the hard non-collinear region of the three-body phase space, and the explicit expressions of $\overline{|M_{ik}^{gb}|^2}$ can be found in Appendix B. In order to avoid introducing external ghost lines while summing over the gluon helicities, we limit ourselves to the sum over the physical polarizations of the gluons [24], i.e.

$$P_i^{\mu\nu} = \sum_T \epsilon_T^\mu(k_i) \epsilon_T^\nu(k_i) = -g^{\mu\nu} + \frac{n_i^\mu k_i^\nu + k_i^\mu n_i^\nu}{n_i \cdot k_i} - \frac{n_i^2 k_i^\mu k_i^\nu}{(n_i \cdot k_i)^2}, \quad (3.17)$$

where the index i ($=1,2$) labels the two external gluons, and $n_i \neq k_i$ is an arbitrary vector.

This polarization sum obeys the transversality relations

$$k_{i\mu} P^{\mu\nu} = P^{\mu\nu} k_{i\nu} = n_{i\mu} P^{\mu\nu} = P^{\mu\nu} n_{i\nu} = 0. \quad (3.18)$$

In the next two subsections, we will discuss in detail the soft and hard collinear gluon emission.

1. Soft gluon emission

In the limit that the energy of the emitted gluon becomes small, i.e. $E_3 \leq \delta_s \sqrt{s}/2$, the matrix element squared $\overline{|M_{ik}^R|^2}$ can be simply factorized into the Born matrix element squared times an eikonal factor Φ_{eik} :

$$\overline{|M_{ik}^R(gb \rightarrow \tilde{t}_i \tilde{\chi}_k^- + g)|^2} \xrightarrow{soft} (4\pi\alpha_s \mu_r^{2\epsilon}) \overline{|M_{ik}^B|^2} \Phi_{eik}, \quad (3.19)$$

where the eikonal factor Φ_{eik} is given by

$$\Phi_{eik} = N \frac{p_a \cdot p_1}{(p_a \cdot p_3)(p_1 \cdot p_3)} + N \frac{p_a \cdot p_b}{(p_b \cdot p_3)(p_a \cdot p_3)} - C_F \frac{m_{\tilde{t}_i}^2}{(p_1 \cdot p_3)^2} - \frac{1}{N} \frac{p_b \cdot p_1}{(p_1 \cdot p_3)(p_b \cdot p_3)}. \quad (3.20)$$

Moreover, the phase space in the soft limit can also be factorized as

$$d\overline{\Gamma}_3(gb \rightarrow \tilde{t}_i \tilde{\chi}_k^- + g) \xrightarrow{soft} d\overline{\Gamma}_2(gb \rightarrow \tilde{t}_i \tilde{\chi}_k^-) dS, \quad (3.21)$$

where dS is the integration over the phase space of the soft gluon, which is given by [25]

$$dS = \frac{1}{2(2\pi)^{3-2\epsilon}} \int_0^{\delta_s \sqrt{s}/2} dE_3 E_3^{1-2\epsilon} d\Omega_{2-2\epsilon}. \quad (3.22)$$

Then the parton level cross section in the soft region can be expressed as

$$\hat{\sigma}_{ik}^S = (4\pi\alpha_s\mu_r^{2\epsilon}) \int d\Gamma_2 \overline{|M_{ik}^B|^2} \int dS \Phi_{eik}. \quad (3.23)$$

Using the approach of Ref. [25], after the integration over the soft gluon phase space, Eq. (3.23) becomes

$$\hat{\sigma}_{ik}^S = \hat{\sigma}^B \left[\frac{\alpha_s}{2\pi} \frac{\Gamma(1-\epsilon)}{\Gamma(1-2\epsilon)} \left(\frac{4\pi\mu_r^2}{s} \right)^\epsilon \right] \left(\frac{A_2^s}{\epsilon^2} + \frac{A_1^s}{\epsilon} + A_0^s \right) \quad (3.24)$$

with

$$\begin{aligned} A_2^s &= \frac{13}{3}, \\ A_1^s &= -2A_2^s \ln \delta_s + \frac{4}{3} + \frac{1}{3} \ln \frac{-u_1}{m_{\tilde{t}_i}^2} - 3 \ln \frac{-t_1}{m_{\tilde{t}_i}^2} + \frac{4}{3} \ln \frac{s}{m_{\tilde{t}_i}^2}, \\ A_0^s &= 2A_2^s \ln^2 \delta_s - 2A_1^s \ln \delta_s + (C_F \frac{\gamma}{\beta} - \frac{1}{4}) \ln \frac{\gamma + \beta}{\gamma - \beta} + \frac{1}{2} \ln^2 \frac{s(\beta - \gamma)}{t_1} + \text{Li}_2 \left[1 + \frac{t_1}{s(\gamma - \beta)} \right] \\ &\quad - \text{Li}_2 \left[1 + \frac{s(\gamma + \beta)}{t_1} \right] + \frac{1}{6} \left\{ \ln^2 \frac{s(\beta - \gamma)}{u_1} - \frac{1}{2} \ln^2 \frac{\gamma + \beta}{\gamma - \beta} + 2 \text{Li}_2 \left[\frac{t_1 + s(\beta + \gamma)}{s(\beta - \gamma)} \right] \right. \\ &\quad \left. - 2 \text{Li}_2 \left[\frac{t_1 + s(\beta - \gamma)}{-u_1} \right] \right\}, \end{aligned}$$

where $\gamma = (s + m_{\tilde{t}_i}^2 - m_{\tilde{\chi}_k^-}^2)/(2s)$ and $\beta = \sqrt{\gamma^2 - m_{\tilde{t}_i}^2/s}$.

2. Hard collinear gluon emission

In the hard collinear region, i.e. $E_3 > \delta_s \sqrt{s}/2$ and $0 < -t' (-u') < \delta_c s$, the emitted hard gluon is collinear to one of the incoming partons. As a consequence of the factorization theorems [27], the squared matrix element for $gb \rightarrow \tilde{t}_i \tilde{\chi}_k^- + g$ can be factorized into the product of the Born squared matrix element and the Altarelli-Parisi splitting function for $b \rightarrow bg$ and $g \rightarrow gg$ [28, 29], i.e.

$$\overline{|M_{ik}^R(gb \rightarrow \tilde{t}_i \tilde{\chi}_k^- + g)|^2} \xrightarrow{\text{collinear}} (4\pi\alpha_s\mu_r^{2\epsilon}) \overline{|M_{ik}^B|^2} \left(\frac{-2P_{bb}(z, \epsilon)}{zt'} + \frac{-2P_{gg}(z, \epsilon)}{zu'} \right), \quad (3.25)$$

where z denotes the fraction of incoming parton $b(g)$'s momentum carried by parton $b(g)$ with the emitted gluon taking a fraction $(1-z)$, and $P_{ij}(z, \epsilon)$ are the unregulated splitting functions in $n = 4 - 2\epsilon$ dimensions for $0 < z < 1$, which can be related to the usual Altarelli-Parisi splitting kernels [28] as $P_{ij}(z, \epsilon) = P_{ij}(z) + \epsilon P'_{ij}(z)$, explicitly

$$\begin{aligned} P_{qq}(z) &= C_F \frac{1+z^2}{1-z}, & P'_{qq}(z) &= -C_F(1-z), \\ P_{gg}(z) &= 2N \left[\frac{z}{1-z} + \frac{1-z}{z} + z(1-z) \right], & P'_{gg}(z) &= 0. \end{aligned} \quad (3.26)$$

Moreover, the three-body phase space also can be factorized in the collinear limit, and, for example, in the limit $0 < -t' < \delta_c s$ it has the following form [25]:

$$d\Gamma_3(gb \rightarrow \tilde{t}_i \tilde{\chi}_k^- + g) \xrightarrow{\text{collinear}} d\Gamma_2(gb \rightarrow \tilde{t}_i \tilde{\chi}_k^-; s' = zs) \frac{(4\pi)^\epsilon}{16\pi^2 \Gamma(1-\epsilon)} dz dt' [-(1-z)t']^{-\epsilon} \quad (3.27)$$

Note that the two-body phase space should be evaluated at a squared parton-parton energy of zs . Then the three-body cross section in the hard collinear region is given by [25]

$$d\sigma_{ik}^{HC} = d\hat{\sigma}_{ik}^B \left[\frac{\alpha_s}{2\pi} \frac{\Gamma(1-\epsilon)}{\Gamma(1-2\epsilon)} \left(\frac{4\pi\mu_r^2}{s} \right)^\epsilon \right] \left(-\frac{1}{\epsilon} \right) \delta_c^{-\epsilon} [P_{bb}(z, \epsilon) G_{b/p}(x_1/z) G_{g/p}(x_2) + P_{gg}(z, \epsilon) G_{g/p}(x_1/z) G_{b/p}(x_2) + (x_1 \leftrightarrow x_2)] \frac{dz}{z} \left(\frac{1-z}{z} \right)^{-\epsilon} dx_1 dx_2, \quad (3.28)$$

where $G_{b(g)/p}(x)$ is the bare PDF.

C. Final States with an Additional Massless Quark

In addition to the real gluon emission, other real emission corrections to the inclusive cross section for $pp \rightarrow \tilde{t}_i \tilde{\chi}_k^-$ at NLO involve the processes with an additional massless (anti)quark in the final states, as shown in Fig.5 ($q = u, d, s, c$):

$$g(p_a) + g(p_b) \rightarrow \tilde{t}_i(p_1) + \tilde{\chi}_k^-(p_2) + \bar{b}(p_3), \quad (3.29)$$

$$q/\bar{q}(p_a) + b(p_b) \rightarrow \tilde{t}_i(p_1) + \tilde{\chi}_k^-(p_2) + q/\bar{q}(p_3), \quad (3.30)$$

$$b/\bar{b}(p_b) + b(p_a) \rightarrow \tilde{t}_i(p_1) + \tilde{\chi}_k^-(p_2) + b/\bar{b}(p_3), \quad (3.31)$$

$$q(p_a) + \bar{q}(p_b) \rightarrow \tilde{t}_i(p_1) + \tilde{\chi}_k^-(p_2) + \bar{b}(p_3). \quad (3.32)$$

Since the contributions from the processes (3.29)-(3.31) contain the initial state collinear singularities, we also need to use the two cutoff phase space slicing method [25]. However, we only split the phase space into two regions, because there are no soft divergences here. Thus, according to the approach shown in Ref. [25], the cross sections for the processes with an additional massless (anti)quark in the final states can be expressed as ($q = u, d, s, c, b$)

$$d\sigma_{ik}^{add} = \sum_{(\alpha, \beta)} \hat{\sigma}_{ik}^{\bar{C}}(\alpha\beta \rightarrow \tilde{t}_i \tilde{\chi}_k^- + X) [G_{\alpha/p}(x_1) G_{\beta/p}(x_2) + (x_1 \leftrightarrow x_2)] dx_1 dx_2 + d\hat{\sigma}_{ik}^B \left[\frac{\alpha_s}{2\pi} \frac{\Gamma(1-\epsilon)}{\Gamma(1-2\epsilon)} \left(\frac{4\pi\mu_r^2}{s} \right)^\epsilon \right] \left(-\frac{1}{\epsilon} \right) \delta_c^{-\epsilon} [P_{bg}(z, \epsilon) G_{g/p}(x_1/z) G_{g/p}(x_2) + \sum_{\alpha=q, \bar{q}} P_{g\alpha}(z, \epsilon) G_{\alpha/p}(x_1/z) G_{b/p}(x_2) + (x_1 \leftrightarrow x_2)] \frac{dz}{z} \left(\frac{1-z}{z} \right)^{-\epsilon} dx_1 dx_2, \quad (3.33)$$

where

$$\begin{aligned}
P_{gq}(z) &= C_F \frac{1 + (1-z)^2}{z}, & P'_{gq}(z) &= -C_F z, \\
P_{qq}(z) &= \frac{1}{2} [z^2 + (1-z)^2], & P'_{qq}(z) &= -z(1-z).
\end{aligned}
\tag{3.34}$$

The first term in Eq.(3.33) represents the non-collinear cross sections for the four processes, and like Eq.(3.16) each $\hat{\sigma}_{ik}^{\bar{C}}$ can be written in the form:

$$d\hat{\sigma}_{ik}^{\bar{C}} = \frac{1}{2s} |\overline{M_{ik}^{\alpha\beta}}|^2 d\bar{\Gamma}_3,
\tag{3.35}$$

where α and β denote the incoming partons in the partonic processes, and $d\bar{\Gamma}_3$ is the three body phase space in the non-collinear region. The explicit expressions of $|\overline{M_{ik}^{\alpha\beta}}|^2$ can be found in Appendix B. The second term in Eq.(3.33) represents the collinear singular cross sections.

Moreover, for the subprocesses $gg/q\bar{q} \rightarrow \tilde{t}_i \tilde{t}_i^* \rightarrow \tilde{t}_i \tilde{\chi}_k^- \bar{b}$ ($q = u, d, s, c, b$), assuming $m_{\tilde{t}_i} > m_{\tilde{\chi}_k^-}$, the stop momentum can approach the stop mass shell, which will lead to singularity arising from the stop propagator. Following the analysis shown in Ref. [4], this problem can easily be solved by introducing the non-zero stop widths $\Gamma_{\tilde{t}_i}$ and regularizing in this way the higher-order amplitudes. However, these on-shell stop contributions are already accounted for by the LO stop pair production with a subsequent decay into a chargino and a bottom quark, and thus should not be considered as a genuine higher order correction to the associated production of top squarks and charginos. Therefore, to avoid double counting, these pole contributions will be subtracted in our numerical calculations below in the same way as shown in Appendix B of Ref. [4].

D. Mass factorization

As mentioned above, after adding the renormalized virtual corrections and the real corrections, the partonic cross sections still contain the collinear divergences, which can be absorbed into the redefinition of the PDF at NLO, in general called mass factorization [23]. This procedure in practice means that first we convolute the partonic cross section with the bare PDF $G_{\alpha/p}(x)$, and then use the renormalized PDF $G_{\alpha/p}(x, \mu_f)$ to replace $G_{\alpha/p}(x)$. In the $\overline{\text{MS}}$ convention, the scale dependent PDF $G_{\alpha/p}(x, \mu_f)$ is given by [25]

$$G_{\alpha/p}(x, \mu_f) = G_{\alpha/p}(x) + \sum_{\beta} \left(-\frac{1}{\epsilon}\right) \left[\frac{\alpha_s}{2\pi} \frac{\Gamma(1-\epsilon)}{\Gamma(1-2\epsilon)} \left(\frac{4\pi\mu_r^2}{\mu_f^2}\right)^\epsilon \right] \int_x^1 \frac{dz}{z} P_{\alpha\beta}(z) G_{\beta/p}(x/z).
\tag{3.36}$$

This replacement will produce a collinear singular counterterm, which is combined with the hard collinear contributions to result in, as the definition in Ref. [25], the $\mathcal{O}(\alpha_s)$ expression for the remaining collinear contribution:

$$\begin{aligned}
d\sigma_{ik}^{coll} &= d\hat{\sigma}_{ik}^B \left[\frac{\alpha_s}{2\pi} \frac{\Gamma(1-\epsilon)}{\Gamma(1-2\epsilon)} \left(\frac{4\pi\mu_r^2}{s} \right)^\epsilon \{ \tilde{G}_{g/p}(x_1, \mu_f) G_{b/p}(x_2, \mu_f) + G_{g/p}(x_1, \mu_f) \tilde{G}_{b/p}(x_2, \mu_f) \right. \\
&\quad + \sum_{\alpha=b,g} \left[\frac{A_1^{sc}(\alpha \rightarrow \alpha g)}{\epsilon} + A_0^{sc}(\alpha \rightarrow \alpha g) \right] G_{g/p}(x_1, \mu_f) G_{b/p}(x_2, \mu_f) \\
&\quad \left. + (x_1 \leftrightarrow x_2) \right\} dx_1 dx_2,
\end{aligned} \tag{3.37}$$

where

$$A_1^{sc}(q \rightarrow qg) = C_F(2 \ln \delta_s + 3/2), \tag{3.38}$$

$$A_1^{sc}(g \rightarrow gg) = 2N \ln \delta_s + (11N - 2n_f)/6, \tag{3.39}$$

$$A_0^{sc} = A_1^{sc} \ln\left(\frac{s}{\mu_f^2}\right), \tag{3.40}$$

$$\tilde{G}_{\alpha/p}(x, \mu_f) = \sum_{\beta} \int_x^{1-\delta_s \delta_{\alpha\beta}} \frac{dy}{y} G_{\beta/p}(x/y, \mu_f) \tilde{P}_{\alpha\beta}(y) \tag{3.41}$$

with

$$\tilde{P}_{\alpha\beta}(y) = P_{\alpha\beta} \ln\left(\delta_c \frac{1-y}{y} \frac{s}{\mu_f^2}\right) - P'_{\alpha\beta}(y). \tag{3.42}$$

Finally, the NLO total cross section for $pp \rightarrow \tilde{t}_i \tilde{\chi}_k^-$ in the \overline{MS} factorization scheme is

$$\begin{aligned}
\sigma_{ik}^{NLO} &= \int \{ dx_1 dx_2 [G_{b/p}(x_1, \mu_f) G_{g/p}(x_2, \mu_f) + x_1 \leftrightarrow x_2] (\hat{\sigma}_{ik}^B + \hat{\sigma}_{ik}^V + \hat{\sigma}_{ik}^S + \hat{\sigma}_{ik}^{\overline{HC}}) + d\sigma_{ik}^{coll} \} \\
&\quad + \sum_{(\alpha,\beta)} \int dx_1 dx_2 [G_{\alpha/p}(x_1, \mu_f) G_{\beta/p}(x_2, \mu_f) + (x_1 \leftrightarrow x_2)] \hat{\sigma}_{ik}^{\overline{C}}(\alpha\beta \rightarrow \tilde{t}_i \tilde{\chi}_k^- + X).
\end{aligned} \tag{3.43}$$

Note that the above expression contains no singularities since $A_2^V + A_2^S = 0$ and $A_1^V + A_1^S + A_1^{sc}(b \rightarrow bg) + A_1^{sc}(g \rightarrow gg) = 0$.

E. Differential Cross section in the Transverse Momentum

In this subsection we present the differential cross section in the transverse momentum p_T of the charginos. Using the notations defined in Ref. [4], the differential distribution with respect to p_T and y for the processes

$$p(P_a) + p(P_b) \rightarrow \tilde{t}_i(p_1) + \tilde{\chi}_k^-(p_2) [+g(p_3)/q(p_3)/\bar{q}(p_3)] \tag{3.44}$$

is given by

$$\frac{d^2\sigma}{dp_T dy} = 2p_T S \sum_{\alpha,\beta} \int_{x_1^-}^1 dx_1 \int_{x_2^-}^1 dx_2 x_1 G_{\alpha/p}(x_1, \mu_f) x_2 G_{\beta/p}(x_2, \mu_f) \frac{d^2\hat{\sigma}_{\alpha\beta}}{dt_2 du_2}, \quad (3.45)$$

where \sqrt{S} is the total center-of-mass energy of the collider, and

$$\begin{aligned} p_T^2 &= \frac{T_2 U_2}{S} - m_{\tilde{\chi}_k^-}^2, & y &= \frac{1}{2} \ln\left(\frac{T_2}{U_2}\right), \\ x_1^- &= \frac{-T_2 - m_{\tilde{\chi}_k^-}^2 + m_{\tilde{t}_i}^2}{S + U_2}, & x_2^- &= \frac{-x_1 U_2 - m_{\tilde{\chi}_k^-}^2 + m_{\tilde{t}_i}^2}{x_1 S + T_2} \end{aligned} \quad (3.46)$$

with $T_2 = (P_b - p_2)^2 - m_{\tilde{\chi}_k^-}^2$ and $U_2 = (P_a - p_2)^2 - m_{\tilde{\chi}_k^-}^2$. The limits of integral over y and p_T are

$$-y^{\max}(p_T) \leq y \leq y^{\max}(p_T), \quad 0 \leq p_T \leq p_T^{\max}, \quad (3.47)$$

with

$$\begin{aligned} y^{\max}(p_T) &= \operatorname{arccosh}\left(\frac{S + m_{\tilde{\chi}_k^-}^2 - m_{\tilde{t}_i}^2}{2\sqrt{S(p_T^2 + m_{\tilde{\chi}_k^-}^2)}}\right), \\ p_T^{\max} &= \frac{1}{2\sqrt{S}} \sqrt{(S + m_{\tilde{\chi}_k^-}^2 - m_{\tilde{t}_i}^2)^2 - 4m_{\tilde{\chi}_k^-}^2 S}. \end{aligned} \quad (3.48)$$

IV. NUMERICAL RESULTS AND CONCLUSION

We now present the numerical results for total and differential cross sections for the associated production of top squarks and charginos at the LHC. In our numerical calculations the Standard Model (SM) parameters were taken to be $\alpha_{ew}(m_W) = 1/128$, $m_W = 80.419$ GeV, $m_Z = 91.1882$ GeV, and $m_t = 174.3$ GeV [30]. We use the two-loop evolution of $\alpha_s(Q)$ [31] ($\alpha_s(M_Z) = 0.118$) and CTEQ6M (CTEQ6L) PDFs [32] throughout the calculations of the NLO (LO) cross sections. Moreover, in order to improve the perturbative calculations, we take the running mass $m_b(Q)$ evaluated by the NLO formula [33]:

$$m_b(Q) = U_6(Q, m_t) U_5(m_t, m_b) m_b(m_b) \quad (4.1)$$

with $m_b(m_b) = 4.25$ GeV [34]. The evolution factor U_f is

$$\begin{aligned} U_f(Q_2, Q_1) &= \left(\frac{\alpha_s(Q_2)}{\alpha_s(Q_1)}\right)^{d^{(f)}} \left[1 + \frac{\alpha_s(Q_1) - \alpha_s(Q_2)}{4\pi} J^{(f)}\right], \\ d^{(f)} &= \frac{12}{33 - 2f}, & J^{(f)} &= -\frac{8982 - 504f + 40f^2}{3(33 - 2f)^2}. \end{aligned} \quad (4.2)$$

In addition, in order to improve the perturbation calculations, especially for large $\tan\beta$, we make the following replacement in the tree-level couplings [33]:

$$m_b(Q) \rightarrow \frac{m_b(Q)}{1 + \Delta m_b}, \quad (4.3)$$

$$\begin{aligned} \Delta m_b = & \frac{2\alpha_s}{3\pi} M_{\tilde{g}} \mu \tan\beta I(m_{\tilde{b}_1}, m_{\tilde{b}_2}, M_{\tilde{g}}) + \frac{h_t^2}{16\pi^2} \mu A_t \tan\beta I(m_{\tilde{t}_1}, m_{\tilde{t}_2}, \mu) \\ & - \frac{g^2}{16\pi^2} \mu M_2 \tan\beta \sum_{i=1}^2 [(R_{i1}^{\tilde{t}})^2 I(m_{\tilde{t}_i}, M_2, \mu) + \frac{1}{2} (R_{i1}^{\tilde{b}})^2 I(m_{\tilde{b}_i}, M_2, \mu)] \end{aligned} \quad (4.4)$$

with

$$I(a, b, c) = \frac{1}{(a^2 - b^2)(b^2 - c^2)(a^2 - c^2)} (a^2 b^2 \log \frac{a^2}{b^2} + b^2 c^2 \log \frac{b^2}{c^2} + c^2 a^2 \log \frac{c^2}{a^2}). \quad (4.5)$$

And, it is necessary for avoiding double counting to subtract these (SUSY-)QCD corrections from the renormalization constant δm_b in the following numerical calculations. The MSSM parameters are determined as follows:

(i) For the parameters M_1 , M_2 and μ in the chargino and neutralino matrices, we take M_2 and μ as the input parameters, and assuming gaugino mass unification we take $M_1 = (5/3) \tan^2 \theta_W M_2$ and $M_{\tilde{g}} = (\alpha_s(M_{\tilde{g}})/\alpha_2) M_2$ [35].

(ii) For the parameters in squark mass matrices, we assume $M_{\tilde{Q}} = M_{\tilde{U}} = M_{\tilde{D}}$ and $A_t = A_b = 300$ GeV to simplify the calculations. Actually, the numerical results are not very sensitive to $A_{t(b)}$.

In our calculations, except in Fig.10, we always choose the renormalization scale $\mu_r = m_{\text{av}}$, and the factorization scale μ_f is fixed to $m_{\text{av}}/3$ instead of m_{av} as mentioned in Sec. I.

Before we discuss in detail the numerical results for associated production of top squarks and charginos at the LHC, in Fig.6 we first show that the following NLO QCD predictions do not depend on the arbitrary cutoffs δ_s and δ_c in the two cutoff phase space slicing method. Here we take $\mu = -200$ GeV, $M_2 = 300$ GeV, $m_{\tilde{t}_1} = 250$ GeV, $\tan\beta = 30$, and $\delta_c = \delta_s/100$. σ_{other} includes the contributions from the Born cross section and the virtual corrections, which are cutoff-independent. We can see that the soft plus hard collinear contributions and the hard non-collinear contributions depend strongly on the cutoffs, and especially for the small cutoffs ($\delta_s < 10^{-4}$) their magnitudes can be ten times larger than the LO total cross section. However, the two contributions ($\sigma_{\text{soft}} + \sigma_{\text{hard/coll}}$ and $\sigma_{\text{hard/non-coll}}$) balance each other very well, and the final result σ_{NLO} is independent of the cutoffs and keeps 0.23 pb. Therefore, we take $\delta_s = 10^{-4}$ and $\delta_c = \delta_s/100$ in the numerical calculations of Fig.7–13.

Fig.7 shows the dependence of the LO and NLO predictions for $pp \rightarrow \tilde{t}_i \tilde{\chi}_k^-$ on $m_{\tilde{t}_1}$, assuming $\mu = -200$ GeV, $M_2 = 300$ GeV and $\tan\beta = 30$, which means that two chargino masses are about 182 GeV and 331 GeV, respectively, and $m_{\tilde{t}_2}$ increases from 342 GeV to 683 GeV for $m_{\tilde{t}_1}$ in the range 100–600 GeV. One finds that the total cross sections for the $\tilde{t}_2 \tilde{\chi}_2^-$ channel are always smallest and less than 3 fb, but the total cross sections for other channels are large and range between 10 fb and several hundred fb for most values of $m_{\tilde{t}_1}$. Especially for the $\tilde{t}_1 \tilde{\chi}_1^-$ channel, the total cross section can reach 1 pb for small values of $m_{\tilde{t}_1}$ ($100 \text{ GeV} < m_{\tilde{t}_1} < 160 \text{ GeV}$), which is almost the same as ones of top quark and charged Higgs boson associated production at the LHC. However, when $m_{\tilde{t}_1}$ get larger and close to $m_{\tilde{t}_2}$, the total cross section for the $\tilde{t}_2 \tilde{\chi}_1^-$ channel is the largest, as shown in Fig.7. Moreover, Fig.7 also shows that the NLO QCD corrections enhance the LO results significantly, which are in general a few ten percent.

In Fig.8 we show the dependence of the LO and NLO predictions for $pp \rightarrow \tilde{t}_i \tilde{\chi}_k^-$ on $m_{\tilde{\chi}_1^-}$, assuming $\mu = -400$ GeV, $m_{\tilde{t}_1} = 250$ GeV and $\tan\beta = 30$, which means that $m_{\tilde{t}_2} = 414$ GeV and $m_{\tilde{\chi}_2^-}$ increases from 417 GeV to 434 GeV for $m_{\tilde{\chi}_1^-}$ in the range 100–300 GeV. One can see that the total cross sections for all channels can exceed 10 fb. For small values of $m_{\tilde{\chi}_1^-}$, the $\tilde{t}_1 \tilde{\chi}_1^-$ channel has the largest total cross sections, and for large values of $m_{\tilde{\chi}_1^-}$, the $\tilde{t}_1 \tilde{\chi}_2^-$ channel has the largest ones, which all can exceed 100 fb. Moreover, Fig.8 also shows that the NLO QCD corrections enhance the LO results, and especially for the $\tilde{t}_1 \tilde{\chi}_1^-$ and $\tilde{t}_2 \tilde{\chi}_1^-$ channels, the enhancement can exceed 50%.

The associated production of \tilde{t}_1 and $\tilde{\chi}_1^-$ is the most important since the total cross sections are the largest for $m_{\tilde{t}_1} < 400$ GeV and $m_{\tilde{\chi}_1^-} < 230$ GeV. Thus we mainly discuss this channel below.

Fig.9 gives the dependence of the K factor (the ratio of the NLO total cross section over the LO one) on $m_{\tilde{t}_1}$ for the $\tilde{t}_1 \tilde{\chi}_1^-$ production. Here we assume the same values of the MSSM parameters as in Fig.7. The K factor contains four contributions: (i) The curve (b) shows the ratio of the improved Born cross section, which is defined as convoluting the LO partonic cross section with the NLO PDFs, over the LO one. The corresponding K factor ranges from 1.18 to 1.39. (ii) The NLO cross section in the curve (c) contains only the contributions from the subprocess with two initial-state gluons, which are positive and the corresponding K factor varies from 0.30 to 0.06. (iii) The NLO cross section in the curve (d) collects only the contributions from massless (anti)quark emission subprocesses as

shown in Eq.(3.30)-(3.32), and the corresponding K factor keeps always about 0.10. (iv) The NLO cross section in the curve (e) includes only the virtual and the real gluon emission corrections, which are negative and the corresponding K factor ranges between -0.36 and -0.29 . Finally, summing above four parts leads to the total K factor as shown in the curve (a), which indicates that the NLO QCD corrections enhance the LO total cross section and vary from 21% to 27%.

In Fig.10 we show the dependence of the total cross sections for the $\tilde{t}_1\tilde{\chi}_1^-$ production on the renormalization/factorization scale, assuming $\mu = -200$ GeV, $M_2 = 300$ GeV, $\tan\beta = 30$, $m_{\tilde{t}_1} = 250$ GeV, and $\mu_r = \mu_f$. One finds that the NLO QCD corrections reduce the dependence significantly. The cross sections vary by $\pm 15\%$ at LO but only by $\pm 4\%$ at NLO in the region $0.5 < \mu_f/m_{\text{av}} < 2.0$. Thus the reliability of the NLO predictions has been improved substantially.

The cross sections of the $\tilde{t}_1\tilde{\chi}_1^-$ production as a function of $\tan\beta$ are displayed for $m_{\tilde{t}_1} = 200, 300$ and 400 GeV in Fig.11, assuming $\mu = -200$ GeV and $M_2 = 300$ GeV. For the dotted curves, Δm_b in Eq.(4.3) is replaced by $\Delta m'_b$ which only includes the corrections of the gluino piece and neglects the rest of the SUSY diagrams in Eq.(4.4). From Fig.11, one can see that the cross sections become large when $\tan\beta$ gets high or low, which is due to the fact that for the coupling $b - \tilde{t}_1 - \tilde{\chi}_1^-$ at low $\tan\beta$ the top quark contribution is enhanced while at high $\tan\beta$ the bottom quark contribution becomes large. Fig.11 also shows that the NLO QCD corrections enhance the LO total cross sections, and for $m_{\tilde{t}_1} = 200$ and 300 GeV, the enhancement is more significant for the medium values of $\tan\beta$ than for the other values. Moreover, after comparing the solid curves with the dotted ones, we can see that the SUSY corrections to Δm_b except the gluino piece decrease the total cross sections significantly, especially for larger values of $\tan\beta$.

Fig.12 shows the dependence of the total cross sections for the $\tilde{t}_1\tilde{\chi}_1^-$ production on the parameters μ and M_2 , assuming $m_{\tilde{t}_1} = 250$ GeV and $\tan\beta = 30$. Note that the phenomenology at CERN e^+e^- LEP and Tevatron [36] has excluded the parameter range $|\mu| \lesssim 180$ GeV, where one chargino mass and one of the neutralino masses can become very small, and especially the latter is zero for vanishing μ . So we focus on the range $|\mu| \gtrsim 180$ GeV. One can see that the cross sections increase with an increase of M_2 for $|\mu| < 450$ GeV, and decrease with an increase of $|\mu|$ except $|\mu| > 350$ GeV for $M_2 = 300$ GeV. The NLO QCD corrections can increase and decrease the LO total cross sections depending on the values of μ and M_2 .

In Fig.13 we display the differential cross sections in the transverse momentum p_T of $\tilde{\chi}_1^-$ for the $\tilde{t}_1\tilde{\chi}_1^-$ production in three cases, which are obtained after integration over all y in Eq.(3.45), assuming $\mu = -200$ GeV and $m_{\tilde{t}_1} = 250$ GeV. In all cases, we find that the NLO QCD corrections enhance the LO differential cross sections for low p_T , but decrease the LO results for high p_T .

In conclusion, we have calculated the NLO inclusive total cross sections for the associated production processes $pp \rightarrow \tilde{t}_i\tilde{\chi}_k^-$ in the MSSM at the LHC. Our calculations show that the total cross sections for the $\tilde{t}_1\tilde{\chi}_1^-$ production for the lighter top squark masses in the region $100 \text{ GeV} < m_{\tilde{t}_1} < 160 \text{ GeV}$ can reach 1 pb in the favorable parameter space allowed by the current precise experiments, and in other cases the total cross sections generally vary from 10 fb to several hundred fb except both $m_{\tilde{t}_1} > 500 \text{ GeV}$ and the $\tilde{t}_2\tilde{\chi}_2^-$ production channel, which means that the LHC may produce abundant events of these processes, and it is very possible to discover these SUSY particles through the above processes in the future experiments, if the supersymmetry exists. Moreover, we find that the NLO QCD corrections in general enhance the LO total cross sections significantly, and vastly reduce the dependence of the total cross sections on the renormalization/factorization scale, which leads to increased confidence in predictions based on these results.

Acknowledgments

We would like to thank T. Plehn, C.-P. Yuan, T.M.P. Tait and M. Klasen for useful discussions and valuable suggestions. This work was supported in part by the National Natural Science Foundation of China.

APPENDIX A

In this appendix, we collect the explicit expressions of the nonzero form factors in Eq.(3.5) and Eq.(3.6). For simplicity, we introduce the following abbreviations for the Passarino-Veltman three-point integrals $C_{i(j)}$ and four-point integrals $D_{i(j)}$, which are defined similar to Ref. [20] except that we take internal masses squared as arguments:

$$C_{i(j)}^a = C_{i(j)}(0, 0, s; 0, 0, 0),$$

$$C_{i(j)}^b = C_{i(j)}(m_{\tilde{t}_i}^2, m_{\tilde{\chi}_k^-}^2, s; 0, m_{\tilde{t}_i}^2, 0),$$

$$\begin{aligned}
C_{i(j)}^c &= C_{i(j)}(t, m_{\tilde{t}_i}^2, 0; m_{\tilde{t}_i}^2, 0, m_{\tilde{t}_i}^2), \\
C_{i(j)}^d &= C_{i(j)}(0, m_{\tilde{t}_i}^2, t; 0, 0, m_{\tilde{t}_i}^2), \\
C_{i(j)}^e &= C_{i(j)}(m_{\tilde{\chi}_k^-}^2, 0, t; m_{\tilde{t}_i}^2, 0, 0), \\
C_{i(j)}^f &= C_{i(j)}(0, 0, s; m_{\tilde{g}}^2, m_{\tilde{g}}^2, m_{\tilde{b}_j}^2), \\
C_{i(j)}^g &= C_{i(j)}(s, 0, 0; m_{\tilde{b}_j}^2, m_{\tilde{g}}^2, m_{\tilde{b}_j}^2), \\
C_{i(j)}^h &= C_{i(j)}(t, m_{\tilde{t}_i}^2, 0; m_{\tilde{g}}^2, m_{\tilde{t}_i}^2, m_{\tilde{g}}^2), \\
C_{i(j)}^i &= C_{i(j)}(t, m_{\tilde{\chi}_k^-}^2, 0; m_{\tilde{g}}^2, m_{\tilde{t}_i}^2, m_{\tilde{b}_j}^2), \\
C_{i(j)}^j &= C_{i(j)}(m_{\tilde{t}_i}^2, m_{\tilde{\chi}_k^-}^2, s; m_{\tilde{g}}^2, m_{\tilde{t}_i}^2, m_{\tilde{b}_j}^2), \\
C_{i(j)}^k &= C_{i(j)}(m_{\tilde{t}_i}^2, 0, u; m_{\tilde{t}_i}^2, m_{\tilde{g}}^2, m_{\tilde{b}_j}^2), \\
D_{i(j)}^a &= D_{i(j)}(m_{\tilde{t}_i}^2, t, 0, s, 0, m_{\tilde{\chi}_k^-}^2; 0, m_{\tilde{t}_i}^2, 0, 0), \\
D_{i(j)}^b &= D_{i(j)}(m_{\tilde{t}_i}^2, u, 0, s, 0, m_{\tilde{\chi}_k^-}^2; 0, m_{\tilde{t}_i}^2, 0, 0), \\
D_{i(j)}^c &= D_{i(j)}(t, m_{\tilde{\chi}_k^-}^2, u, m_{\tilde{t}_i}^2, 0, 0; 0, m_{\tilde{t}_i}^2, 0, m_{\tilde{t}_i}^2), \\
D_{i(j)}^d &= D_{i(j)}(0, t, m_{\tilde{\chi}_k^-}^2, s, m_{\tilde{t}_i}^2, 0; m_{\tilde{g}}^2, m_{\tilde{g}}^2, m_{\tilde{t}_i}^2, m_{\tilde{b}_j}^2), \\
D_{i(j)}^e &= D_{i(j)}(s, m_{\tilde{\chi}_k^-}^2, u, 0, m_{\tilde{t}_i}^2, 0; m_{\tilde{g}}^2, m_{\tilde{b}_j}^2, m_{\tilde{t}_i}^2, m_{\tilde{b}_j}^2), \\
D_{i(j)}^f &= D_{i(j)}(t, m_{\tilde{\chi}_k^-}^2, u, m_{\tilde{t}_i}^2, 0, 0; m_{\tilde{g}}^2, m_{\tilde{t}_i}^2, m_{\tilde{b}_j}^2, m_{\tilde{t}_i}^2).
\end{aligned}$$

Many above functions contain the soft infrared and collinear singularities, but all Passarino-Veltman integrals can be reduced down to the scalar function B_0 , C_0 and D_0 . Here we present the explicit expressions of C_0 and D_0 , which contain the singularities and are used in our calculations:

$$\begin{aligned}
C_0^a &= \frac{C_\epsilon}{s} \left(\frac{1}{\epsilon^2} - \frac{1}{\epsilon} \ln \frac{s}{m_{\tilde{t}_i}^2} + \frac{1}{2} \ln^2 \frac{s}{m_{\tilde{t}_i}^2} - \frac{2\pi^2}{3} \right), \\
C_0^d &= \frac{C_\epsilon}{t_1} \left[\frac{1}{2\epsilon^2} - \frac{1}{\epsilon} \ln \left(\frac{-t_1}{m_{\tilde{t}_i}^2} \right) - \text{Li}_2 \left(\frac{t}{t_1} \right) + \frac{1}{2} \ln^2 \left(\frac{-t_1}{m_{\tilde{t}_i}^2} \right) \right], \\
C_0^e &= \frac{C_\epsilon}{t_2} \left[\frac{1}{\epsilon} \ln \left(\frac{m_{\tilde{\chi}_k^-}^2 - m_{\tilde{t}_i}^2}{t_1} \right) + \text{Li}_2 \left(\frac{m_{\tilde{\chi}_k^-}^2}{m_{\tilde{\chi}_k^-}^2 - m_{\tilde{t}_i}^2} \right) - \text{Li}_2 \left(\frac{t}{t_1} \right) - \frac{1}{2} \ln^2 \left(1 - \frac{m_{\tilde{\chi}_k^-}^2}{m_{\tilde{t}_i}^2} \right) + \frac{1}{2} \ln^2 \left(\frac{-t_1}{m_{\tilde{t}_i}^2} \right) \right], \\
D_0^a &= \frac{C_\epsilon}{st_1} \left[\frac{3}{2\epsilon^2} - \frac{1}{\epsilon} \ln \frac{s}{m_{\tilde{t}_i}^2} + \frac{1}{\epsilon} \ln \frac{m_{\tilde{t}_i}^2 - m_{\tilde{\chi}_k^-}^2}{m_{\tilde{t}_i}^2} - \frac{2}{\epsilon} \ln \frac{-t_1}{m_{\tilde{t}_i}^2} - \frac{\pi^2}{2} - \text{Li}_2 \left(\frac{t}{t_1} \right) + \text{Li}_2 \left(\frac{t_2}{m_{\tilde{t}_i}^2 - m_{\tilde{\chi}_k^-}^2} \right) \right. \\
&\quad \left. - \text{Li}_2 \left(1 + \frac{m_{\tilde{t}_i}^2 - m_{\tilde{\chi}_k^-}^2}{s} \right) + 2\text{Li}_2 \left(-\frac{fb}{st_1} \right) - \frac{1}{2} \ln^2 \frac{m_{\tilde{t}_i}^2 - m_{\tilde{\chi}_k^-}^2}{m_{\tilde{t}_i}^2} + \ln \frac{s}{m_{\tilde{t}_i}^2} \ln \frac{m_{\tilde{t}_i}^2 - m_{\tilde{\chi}_k^-}^2}{m_{\tilde{t}_i}^2} \right]
\end{aligned}$$

$$\begin{aligned}
& + \frac{1}{2} \ln^2 \frac{-t_1}{m_{\tilde{t}_i}^2} + \ln \frac{st_1 + f_b}{st_1} \left(\ln \frac{m_{\tilde{\chi}_k^-}^2 - m_{\tilde{t}_i}^2}{s} - \ln \frac{-t_1}{m_{\tilde{t}_i}^2} \right) - \text{R}(0, 1, -t_1, t_2, 0, -\frac{s}{m_{\tilde{t}_i}^2}) \\
& - \text{R}(0, 1, st_1, f_b, -1, -\frac{t}{t_1}) - \text{R}(0, 1, st_1, f_b, -1, 1 + \frac{m_{\tilde{t}_i}^2 - m_{\tilde{\chi}_k^-}^2}{s})], \\
D_0^b &= D_0^a (t \rightarrow u, t_1 \rightarrow u_1, t_2 \rightarrow u_2), \\
D_0^c &= \frac{C_\epsilon}{u_1 t_1} \left[\frac{1}{2\epsilon^2} - \frac{1}{\epsilon} \ln \frac{-t_1}{m_{\tilde{t}_i}^2} + \frac{1}{\epsilon} \ln \frac{m_{\tilde{t}_i}^2 - m_{\tilde{\chi}_k^-}^2}{m_{\tilde{t}_i}^2} - \frac{1}{\epsilon} \ln \frac{-u_1}{m_{\tilde{t}_i}^2} - \text{Li}_2\left(\frac{t}{t_1}\right) + \text{Li}_2\left(\frac{m_{\tilde{\chi}_k^-}^2}{m_{\tilde{\chi}_k^-}^2 - m_{\tilde{t}_i}^2}\right) \right. \\
& - \text{Li}_2\left(\frac{u}{u_1}\right) - \frac{1}{2} \ln^2 \frac{m_{\tilde{t}_i}^2 - m_{\tilde{\chi}_k^-}^2}{m_{\tilde{t}_i}^2} + \frac{1}{2} \ln^2 \frac{-t_1}{m_{\tilde{t}_i}^2} + \frac{1}{2} \ln^2 \frac{-u_1}{m_{\tilde{t}_i}^2} + \text{R}\left(\frac{u}{m_{\tilde{\chi}_k^-}^2}, 1, \frac{-f_c}{m_{\tilde{\chi}_k^-}^2}, s, 1, -\frac{m_{\tilde{\chi}_k^-}^2}{m_{\tilde{t}_i}^2}\right) \\
& + \text{R}\left(\frac{t}{m_{\tilde{t}_i}^2}, 1, \frac{-f_c}{m_{\tilde{t}_i}^2}, u, 1, -1\right) + \text{R}(0, 1, u_1 t_1, f_c, \frac{m_{\tilde{t}_i}^2 - m_{\tilde{\chi}_k^-}^2}{m_{\tilde{t}_i}^2}, \frac{m_{\tilde{\chi}_k^-}^2}{m_{\tilde{t}_i}^2}) \\
& \left. - \text{R}(0, 1, u_1 t_1, f_c, -\frac{u_1}{m_{\tilde{t}_i}^2}, \frac{u}{m_{\tilde{t}_i}^2}) - \text{R}(0, 1, u_1 t_1, f_c, -\frac{t_1}{m_{\tilde{t}_i}^2}, \frac{t}{m_{\tilde{t}_i}^2}) \right],
\end{aligned}$$

where we define $C_\epsilon = \Gamma(1 + \epsilon)(4\pi\mu_r^2/m_{\tilde{t}_i}^2)^\epsilon$, and

$$\begin{aligned}
f_b &= t(t_1 + u_1) + m_{\tilde{t}_i}^2 (m_{\tilde{t}_i}^2 - m_{\tilde{\chi}_k^-}^2), & f_c &= m_{\tilde{t}_i}^2 m_{\tilde{\chi}_k^-}^2 - tu, \\
\text{R}(x_1, x_2, x_3, x_4, x_5, x_6) &= \text{Li}_2\left(\frac{x_6 x_1'}{\Delta'}\right) - \text{Li}_2\left(\frac{x_6 x_2'}{\Delta'}\right) + \ln \frac{-\Delta'}{x_4} \ln \frac{x_2'}{x_1'}
\end{aligned}$$

with $\Delta' = x_3 x_6 - x_5 x_4$, $x_1' = x_3 + x_1 x_4$, and $x_2' = x_3 + x_2 x_4$.

Moreover, there are the following relations between the form factors ($i = 1 \dots 6$):

$$\begin{aligned}
f_{2i}^\alpha &= f_{2i-1}^\alpha (l_{ik}^{\tilde{t}} \leftrightarrow k_{ik}^{\tilde{t}}, R_{j1}^{\tilde{b}} \leftrightarrow R_{j2}^{\tilde{b}}, R_{i1}^{\tilde{t}} \leftrightarrow R_{i2}^{\tilde{t}}), \\
f_{2i}^{\text{Box}(\beta)} &= f_{2i-1}^{\text{Box}(\beta)} (l_{ik}^{\tilde{t}} \leftrightarrow k_{ik}^{\tilde{t}}, R_{j1}^{\tilde{b}} \leftrightarrow R_{j2}^{\tilde{b}}, R_{i1}^{\tilde{t}} \leftrightarrow R_{i2}^{\tilde{t}}).
\end{aligned}$$

Thus we will only present the explicit expressions of f_{2i-1}^α and $f_{2i-1}^{\text{Box}(\beta)}$.

For the diagram (a) in Fig.2, we find

$$\begin{aligned}
f_1^a &= -3m_{\tilde{g}} C_0^f R_{j1}^{\tilde{b}} R_{j2}^{\tilde{b}} k_{ik}^{\tilde{t}}, \\
f_3^a &= \frac{1}{6s} l_{ik}^{\tilde{t}} \{ (9 - 2\epsilon) B_0(s, 0, 0) - 40(1 - 2\epsilon) C_{00}^a + 18s C_0^a + (R_{j1}^{\tilde{b}})^2 [36C_{00}^f + 4C_{00}^g] \\
& - 18B_0(s, m_{\tilde{g}}^2, m_{\tilde{b}_j}^2) \}, \\
f_5^a &= 2f_3^a + \frac{1}{3s} l_{ik}^{\tilde{t}} \{ s(7C_1^a - 2C_0^a - 20(1 - \epsilon)(C_{12}^a + C_{22}^a + C_2^a) + 16C_2^a) + (R_{j1}^{\tilde{b}})^2 [2C_0^g (m_{\tilde{b}_j}^2 \\
& - m_{\tilde{g}}^2) + 2B_0(s, m_{\tilde{g}}^2, m_{\tilde{b}_j}^2) - 2B_0(0, m_{\tilde{b}_j}^2, m_{\tilde{b}_j}^2) + 2s(C_0^g + C_{11}^g + C_{12}^g + 2C_1^g + 9C_2^f + C_2^g \\
& + 9C_{12}^f + 9C_{22}^f) \}, \\
f_9^a &= -\frac{2}{s} f_1^a + \frac{2}{3s} m_{\tilde{g}} (C_1^g + 9C_2^f) R_{j1}^{\tilde{b}} R_{j2}^{\tilde{b}} k_{ik}^{\tilde{t}}.
\end{aligned}$$

For the diagram (b) in Fig.2, we find

$$\begin{aligned}
f_1^b &= \frac{4}{3} \{ 2l_{jk}^{\bar{b}} R_{j1}^{\bar{b}} [m_t R_{i2}^{\bar{t}} (C_1^j + C_2^j) - m_{\bar{g}} R_{i1}^{\bar{t}} (C_0^j + C_1^j + C_2^j)] - m_{\bar{\chi}_k^-} [l_{ik}^{\bar{t}} (2C_0^b + C_1^b + 2C_2^b) \\
&\quad - 2k_{jk}^{\bar{b}} R_{j1}^{\bar{b}} R_{i2}^{\bar{t}} C_2^j] \}, \\
f_3^b &= \frac{4}{3s} \{ l_{ik}^{\bar{t}} [B_0(m_{\bar{\chi}_k^-}^2, 0, m_{\bar{t}_i}^2) - 2B_0(s, 0, 0) - s_{\Delta} (2C_0^b + C_1^b + C_2^b) + m_{\bar{t}_i}^2 (C_1^b - 2C_0^b + C_2^b) \\
&\quad - m_{\bar{\chi}_k^-}^2 C_2^b] + 2k_{jk}^{\bar{t}} R_{j1}^{\bar{b}} [m_t m_{\bar{g}} R_{i1}^{\bar{t}} C_0^j + R_{i2}^{\bar{t}} (B_0(m_{\bar{\chi}_k^-}^2, m_t^2, m_{\bar{b}_j}^2) + m_{\bar{g}}^2 C_0^j + m_{\bar{t}_i}^2 (C_1^j + C_2^j))] \\
&\quad - 2(t_2 + u_2 + m_{\bar{\chi}_k^-}^2) [l_{ik}^{\bar{t}} (2C_0^b + C_1^b + 2C_2^b) - 2k_{jk}^{\bar{b}} R_{j1}^{\bar{b}} R_{i2}^{\bar{t}} C_2^j] + 2m_{\bar{\chi}_k^-} l_{jk}^{\bar{b}} R_{j1}^{\bar{b}} [m_{\bar{g}} R_{i1}^{\bar{t}} (C_0^j \\
&\quad + C_1^j) - m_t R_{i2}^{\bar{t}} C_1^j] \}, \\
f_5^b &= 2f_3^b.
\end{aligned}$$

For the diagram (c) in Fig.2, we find

$$\begin{aligned}
f_1^c &= -\frac{8}{3s} l_{ik}^{\bar{t}} m_{\bar{g}} R_{j1}^{\bar{b}} R_{j2}^{\bar{b}} B_0(s, m_{\bar{g}}^2, m_{\bar{b}_j}^2), \\
f_3^c &= -\frac{4}{3s} l_{ik}^{\bar{t}} [2(1 - \epsilon) B_1(s, 0, 0) + 2(R_{j1}^{\bar{b}})^2 B_1(s, m_{\bar{g}}^2, m_{\bar{b}_j}^2)], \\
f_5^c &= 2f_3^c.
\end{aligned}$$

For the diagram (d) in Fig.2, we find

$$\begin{aligned}
f_5^d &= \frac{1}{12} \left\{ \frac{l_{ik}^{\bar{t}}}{t_1} [16B_0(t, 0, m_{\bar{t}_i}^2) + 16B_0(m_{\bar{t}_i}^2, 0, m_{\bar{t}_i}^2) + t_1(18C_0^d - 2C_1^c + 27C_2^d) - 8m_{\bar{t}_i}^2 (C_1^c - 9C_2^d)] \right. \\
&\quad - \frac{4l_{jk}^{\bar{t}} R_{i1}^{\bar{t}}}{t - m_{\bar{t}_j}} [8R_{j1}^{\bar{t}} (B_0(t, m_{\bar{g}}^2, m_{\bar{t}_i}^2) + B_0(m_{\bar{t}_i}^2, m_{\bar{g}}^2, m_{\bar{t}_i}^2)) - (R_{j1}^{\bar{t}} (2m_{\bar{g}}^2 + 2m_t^2 - t - m_{\bar{t}_i}^2) \\
&\quad \left. - 4m_{\bar{g}} m_t R_{j2}^{\bar{t}}) (9C_1^h - C_1(t, m_{\bar{t}_i}^2, 0; m_{\bar{t}_i}^2, m_{\bar{g}}^2, m_{\bar{t}_i}^2))] \right\} + (R_{i1}^{\bar{t}} \leftrightarrow R_{i2}^{\bar{t}}, R_{j1}^{\bar{t}} \leftrightarrow R_{j2}^{\bar{t}}), \\
f_7^d &= -f_5^d.
\end{aligned}$$

For the diagram (e) in Fig.2, we find

$$\begin{aligned}
f_5^e &= \frac{8}{3t_1} \{ l_{ik}^{\bar{t}} [B_0(m_{\bar{\chi}_k^-}^2, 0, m_{\bar{t}_i}^2) - t_2 (C_0^e + C_1^e + C_2^e) - 2m_{\bar{t}_i}^2 C_0^e - 2m_{\bar{\chi}_k^-}^2 (C_1^e + C_2^e)] \\
&\quad - 2R_{i1}^{\bar{t}} R_{j1}^{\bar{b}} [k_{jk}^{\bar{b}} (B_0(m_{\bar{\chi}_k^-}^2, m_{\bar{t}_i}^2, m_{\bar{b}_j}^2) + m_{\bar{g}}^2 C_0^i + t_2 C_1^i + m_{\bar{\chi}_k^-}^2 C_1^i) - l_{jk}^{\bar{b}} m_{\bar{\chi}_k^-} m_{\bar{g}} (C_0^i + C_1^i)] \\
&\quad + 2R_{i2}^{\bar{t}} R_{j1}^{\bar{b}} m_t (k_{jk}^{\bar{b}} m_{\bar{g}} C_0^i - l_{jk}^{\bar{b}} m_{\bar{\chi}_k^-} C_1^i) \}, \\
f_7^e &= -f_5^e.
\end{aligned}$$

For the diagram (f) in Fig.2, we find

$$\begin{aligned}
f_5^f &= -\frac{8}{3t_1} \left\{ \frac{l_{ik}^{\bar{t}}}{t_1} [2(t + m_{\bar{t}_i}^2) B_0(t, 0, m_{\bar{t}_i}^2) - A_0(m_{\bar{t}_i}^2)] + \frac{4l_{jk}^{\bar{t}}}{t - m_{\bar{t}_j}^2} [(tB_1 + A_0(m_{\bar{t}_i}^2) + m_{\bar{g}}^2 B_0) (R_{i1}^{\bar{t}} R_{j1}^{\bar{t}} \right. \\
&\quad \left. + R_{i2}^{\bar{t}} R_{j2}^{\bar{t}}) - m_t m_{\bar{g}} (R_{i2}^{\bar{t}} R_{j1}^{\bar{t}} + R_{i1}^{\bar{t}} R_{j2}^{\bar{t}}) B_0] (t, m_{\bar{g}}^2, m_{\bar{t}_i}^2) \right\}, \\
f_7^f &= -f_5^f.
\end{aligned}$$

For the box diagram (a) in Fig.3, we find

$$\begin{aligned}
f_1^{\text{Box}(a)} &= \frac{3}{2t_2} \tilde{l}_{ik}^- m_{\tilde{\chi}_k^-} [B_0(m_{\tilde{\chi}_k^-}^2, 0, m_{\tilde{t}_i}^2) - B_0(t, 0, m_{\tilde{t}_i}^2) + t_2(C_1^b + 4D_{00}^a - 2t_1 D_1^a)], \\
f_3^{\text{Box}(a)} &= -\frac{3}{2} \tilde{l}_{ik}^- [C_0^a + C_0^b + C_1^a + C_1^b + C_2^a + C_2^b + 4D_{00}^a - 2t_1(D_0^a + D_1^a + D_2^a + D_3^a)], \\
f_5^{\text{Box}(a)} &= \frac{3}{2t_2} \tilde{l}_{ik}^- \{2B_0(m_{\tilde{\chi}_k^-}^2, 0, m_{\tilde{t}_i}^2) - 2B_0(t, 0, m_{\tilde{t}_i}^2) - t_2[2C_0^a + 2C_0^e + C_1^b + 2C_1^e - 2C_2^a + C_2^b \\
&\quad + 6D_{00}^a + s(D_{11}^a + 5D_{13}^a + 2D_1^a + 4D_{33}^a + 4D_3^a) - s_\Delta(D_{11}^a + 2D_{13}^a + 2D_1^a + D_{33}^a + 2D_3^a) \\
&\quad - t_1(2D_0^a + 3D_{12}^a + 3D_1^a + 3D_{23}^a + 2D_2^a + 3D_3^a) + u_2(2D_0^a + D_{11}^a - 3D_{12}^a + D_{13}^a + 3D_1^a \\
&\quad - 3D_{23}^a - 2D_2^a + D_3^a)] - t_2 m_{\tilde{t}_i}^2 (2D_{11}^a + D_{13}^a - 4D_1^a - D_{33}^a - 6D_3^a) + t_2 m_{\tilde{\chi}_k^-}^2 (D_{13}^a + D_{33}^a \\
&\quad - 2D_3^a)\}, \\
f_7^{\text{Box}(a)} &= -\frac{3}{2t_2} \tilde{l}_{ik}^- \{4B_0(m_{\tilde{\chi}_k^-}^2, 0, m_{\tilde{t}_i}^2) - 4B_0(t, 0, m_{\tilde{t}_i}^2) + t_2[2C_0^b - 4C_0^e + C_1^b - s(4D_{13}^a + 2D_{11}^a \\
&\quad + D_{11}^a) + s_\Delta(D_{13}^a + 2D_1^a - 2D_3^a + D_{11}^a) - t_1(D_1^a - 2D_2^a) - u_2(3D_1^a - 2D_2^a + D_{11}^a) \\
&\quad - (2D_0^a - 3D_{12}^a)(t_1 + u_2)] - t_2 m_{\tilde{t}_i}^2 (2D_{11}^a - D_{13}^a - 4D_1^a + 2D_3^a) + t_2 m_{\tilde{\chi}_k^-}^2 (D_{13}^a - 2D_3^a)\}, \\
f_9^{\text{Box}(a)} &= 6\tilde{l}_{ik}^- m_{\tilde{\chi}_k^-} (D_{12}^a + D_{13}^a + D_{23}^a + D_{33}^a + D_3^a), \\
f_{11}^{\text{Box}(a)} &= -6\tilde{l}_{ik}^- m_{\tilde{\chi}_k^-} (D_{12}^a + D_{13}^a).
\end{aligned}$$

For the box diagram (b) in Fig.3, we find

$$\begin{aligned}
f_1^{\text{Box}(b)} &= -\frac{1}{6} \tilde{l}_{ik}^- m_{\tilde{\chi}_k^-} (2C_0^b + C_1^b - 4D_{00}^b), \\
f_3^{\text{Box}(b)} &= \frac{1}{6} \tilde{l}_{ik}^- [2C_0^a + 2C_0^b - C_0(u, m_{\tilde{\chi}_k^-}^2, 0; 0, m_{\tilde{t}_i}^2, 0) + C_1^b + C_2^b - 4D_{00}^b + (t + m_{\tilde{\chi}_k^-}^2) D_3^b \\
&\quad - 2u_1 D_0^b - (u_1 + 2m_{\tilde{t}_i}^2)(D_1^b + D_3^b)], \\
f_5^{\text{Box}(b)} &= \frac{1}{3} \tilde{l}_{ik}^- [2(C_0^a + C_1^a + C_2^a - D_{00}^b) + (s + t_2)(2D_0^b + D_{11}^b + D_{12}^b + 3D_1^b + 2D_2^b + D_3^b) \\
&\quad - s(D_{23}^b + D_{33}^b) + t_2(D_{13}^b + D_3^b) - 2m_{\tilde{t}_i}^2 (D_{11}^b + D_{12}^b + D_{13}^b + D_1^b)], \\
f_7^{\text{Box}(b)} &= \frac{1}{3} \tilde{l}_{ik}^- [2C_0^b + C_1^b + C_1(u, m_{\tilde{\chi}_k^-}^2, 0; 0, m_{\tilde{t}_i}^2, 0) + u_1(D_{11}^b + 2D_1^b) + 2m_{\tilde{t}_i}^2 D_{11}^b], \\
f_9^{\text{Box}(b)} &= \frac{2}{3} \tilde{l}_{ik}^- m_{\tilde{\chi}_k^-} (D_{13}^b + D_{23}^b + D_{33}^b + D_3^b), \\
f_{11}^{\text{Box}(b)} &= -\frac{2}{3} \tilde{l}_{ik}^- m_{\tilde{\chi}_k^-} D_{13}^b.
\end{aligned}$$

For the box diagram (c) in Fig.3, we find

$$\begin{aligned}
f_1^{\text{Box}(c)} &= -m_{\tilde{\chi}_k^-} f_3^{\text{Box}(c)} = -\frac{2}{3} m_{\tilde{\chi}_k^-} \tilde{l}_{ik}^- D_{00}^c, \\
f_5^{\text{Box}(c)} &= -\frac{1}{3t_2} \tilde{l}_{ik}^- \{2B_0(m_{\tilde{\chi}_k^-}^2, 0, m_{\tilde{t}_i}^2) - 2B_0(t, 0, m_{\tilde{t}_i}^2) + t_2[-2C_0^e - 2C_1^e + 2D_{00}^c + (s + 2t
\end{aligned}$$

$$\begin{aligned}
& +2u_2)(D_{13}^c + D_1^c) + 2u(D_{13}^c + D_3^c + D_{23}^c + D_{33}^c) + u_1(2D_0^c + 3D_1^c - D_{23}^c + 2D_2^c \\
& - D_{33}^c + D_3^c) + D_{12}^c(t + m_{\tilde{\chi}_k^-}^2 - 2u_2) + D_{11}^c(t + u + u_2)\}, \\
f_7^{\text{Box}(c)} &= \frac{1}{3t_2} l_{ik}^{\tilde{t}} \{2B_0(m_{\tilde{\chi}_k^-}^2, 0, m_{\tilde{t}_i}^2) - 2B_0(t, 0, m_{\tilde{t}_i}^2) + t_2[-2C_0^e + sD_1^c + (t_1 + u_2)(2D_1^c + D_{11}^c \\
& + D_{13}^c) + (C_0 + C_1 + C_2)(m_{\tilde{\chi}_k^-}^2, 0, u; 0, m_{\tilde{t}_i}^2, m_{\tilde{t}_i}^2) + u_1(2D_0^c + 3D_1^c + D_{11}^c + 2D_{13}^c \\
& + D_{33}^c + 3D_3^c) + 2m_{\tilde{\chi}_k^-}^2(D_{11}^c + 2D_{13}^c + D_1^c + D_{33}^c + D_3^c)]\}, \\
f_9^{\text{Box}(c)} &= -\frac{2}{3} l_{ik}^{\tilde{t}} m_{\tilde{\chi}_k^-} (D_{11}^c + D_{12}^c + D_{13}^c + D_1^c), \\
f_{11}^{\text{Box}(c)} &= \frac{2}{3} l_{ik}^{\tilde{t}} m_{\tilde{\chi}_k^-} (D_{11}^c + D_{13}^c + D_1^c).
\end{aligned}$$

For the box diagram (d) in Fig.3, we find

$$\begin{aligned}
f_1^{\text{Box}(d)} &= 3R_{j1}^{\tilde{b}} \{k_{jk}^{\tilde{b}} m_{\tilde{\chi}_k^-} R_{i2}^{\tilde{t}} (C_0^j + C_1^i - 2D_{00}^d + t_1 D_2^d) + l_{jk}^{\tilde{b}} [m_{\tilde{g}} R_{i1}^{\tilde{t}} (C_0^i - C_0^j + 2D_{00}^d + t_1 D_0^d \\
& + u_2 D_0^d + u_2 D_2^d) + m_t R_{i2}^{\tilde{t}} (C_0^j - 2D_{00}^d - u_2 D_2^d)]\}, \\
f_3^{\text{Box}(d)} &= 3R_{j1}^{\tilde{b}} \{l_{jk}^{\tilde{b}} m_{\tilde{\chi}_k^-} [m_{\tilde{g}} R_{i1}^{\tilde{t}} (D_0^d + D_2^d) - m_t R_{i2}^{\tilde{t}} D_2^d] + k_{jk}^{\tilde{b}} [m_t m_{\tilde{g}} R_{i1}^{\tilde{t}} D_0^d - R_{i2}^{\tilde{t}} (C_0^j - 2D_{00}^d \\
& + m_{\tilde{g}}^2 D_0^d + t D_2^d)]\}, \\
f_5^{\text{Box}(d)} &= -6R_{j1}^{\tilde{b}} \{l_{jk}^{\tilde{b}} m_{\tilde{\chi}_k^-} [m_{\tilde{g}} R_{i1}^{\tilde{t}} (D_{12}^d + D_1^d + D_{22}^d + D_2^d) - m_t R_{i2}^{\tilde{t}} (D_{12}^d + D_{22}^d)] \\
& + k_{jk}^{\tilde{b}} [m_t m_{\tilde{g}} R_{i1}^{\tilde{t}} (D_1^d + D_2^d) + R_{i2}^{\tilde{t}} (C_0^j - 2D_{00}^d - m_{\tilde{g}}^2 (D_1^d + D_2^d) + (t_1 + u_2)(D_{11}^d + D_{12}^d \\
& + D_{13}^d + D_1^d + D_{23}^d) + t_1 D_2^d - m_{\tilde{t}_i}^2 (D_{12}^d + D_{22}^d)]\}, \\
f_7^{\text{Box}(d)} &= 6R_{j1}^{\tilde{b}} \{l_{jk}^{\tilde{b}} m_{\tilde{\chi}_k^-} [m_{\tilde{g}} R_{i1}^{\tilde{t}} (D_{22}^d + D_2^d) - m_t R_{i2}^{\tilde{t}} D_{22}^d] + k_{jk}^{\tilde{b}} [m_t m_{\tilde{g}} R_{i1}^{\tilde{t}} D_2^d - R_{i2}^{\tilde{t}} (C_1^i \\
& + m_{\tilde{g}}^2 D_2^d - t_1 (D_{12}^d + D_{23}^d) - u_2 (D_{12}^d + D_{23}^d) + m_{\tilde{t}_i}^2 D_{22}^d)]\}, \\
f_9^{\text{Box}(d)} &= 6R_{j1}^{\tilde{b}} \{l_{jk}^{\tilde{b}} [m_{\tilde{g}} R_{i1}^{\tilde{t}} (D_0^d + D_{11}^d + 2D_{12}^d + D_{13}^d + 2D_1^d + D_{22}^d + D_{23}^d + 2D_2^d) \\
& - m_t R_{i2}^{\tilde{t}} (D_{11}^d + 2D_{12}^d + D_{13}^d + D_1^d + D_{22}^d + D_{23}^d + D_2^d)] - k_{jk}^{\tilde{b}} m_{\tilde{\chi}_k^-} R_{i2}^{\tilde{t}} (D_{11}^d \\
& + D_{12}^d + D_{13}^d + D_1^d + D_{23}^d)\}, \\
f_{11}^{\text{Box}(d)} &= 6R_{j1}^{\tilde{b}} \{l_{jk}^{\tilde{b}} [m_t R_{i2}^{\tilde{t}} (D_{12}^d + D_{22}^d + D_{23}^d) - m_{\tilde{g}} R_{i1}^{\tilde{t}} (D_{12}^d + D_{22}^d + D_{23}^d + D_2^d)] \\
& + k_{jk}^{\tilde{b}} m_{\tilde{\chi}_k^-} R_{i2}^{\tilde{t}} (D_{12}^d + D_{23}^d)\}.
\end{aligned}$$

For the box diagram (e) in Fig.3, we find

$$\begin{aligned}
f_1^{\text{Box}(e)} &= -\frac{2}{3} R_{j1}^{\tilde{b}} [k_{jk}^{\tilde{b}} m_{\tilde{\chi}_k^-} R_{i2}^{\tilde{t}} + l_{jk}^{\tilde{b}} (m_t R_{i2}^{\tilde{t}} - m_{\tilde{g}} R_{i1}^{\tilde{t}})] D_{00}^e, \\
f_3^{\text{Box}(e)} &= \frac{2}{3} k_{jk}^{\tilde{b}} R_{j1}^{\tilde{b}} R_{i2}^{\tilde{t}} D_{00}^e, \\
f_5^{\text{Box}(e)} &= \frac{2}{3} R_{j1}^{\tilde{b}} \{l_{jk}^{\tilde{b}} m_{\tilde{\chi}_k^-} [(R_{i2}^{\tilde{t}} m_t - m_{\tilde{g}} R_{i1}^{\tilde{t}}) (D_{22}^e + D_{12}^e + D_{23}^e + D_2^e) - m_{\tilde{g}} R_{i1}^{\tilde{t}} (D_0^e + D_1^e
\end{aligned}$$

$$\begin{aligned}
& + D_2^e + D_3^e)] + k_{jk}^{\bar{b}} [R_{i2}^{\bar{t}} (2D_{00}^e + m_{\bar{t}_i}^2 (D_{12}^e + D_{22}^e + D_{23}^e + D_2^e)) + s(D_{12}^e + D_{11}^e \\
& + D_{13}^e + D_1^e) + m_{\bar{g}} (R_{i2}^{\bar{t}} m_{\bar{g}} - R_{i1}^{\bar{t}} m_t) (D_0^e + D_1^e + D_2^e + D_3^e)]], \\
f_7^{\text{Box}(e)} &= \frac{2}{3} R_{j1}^{\bar{b}} \{ l_{jk}^{\bar{b}} m_{\bar{\chi}_k^-} [m_{\bar{g}} R_{i1}^{\bar{t}} (D_{22}^e + D_2^e) - m_t R_{i2}^{\bar{t}} D_{22}^e] + k_{jk}^{\bar{b}} [m_{\bar{g}} m_t R_{i1}^{\bar{t}} D_2^e + R_{i2}^{\bar{t}} ((C_0 \\
& + C_1 + C_2) (m_{\bar{\chi}_k^-}^2, 0, u; m_t^2, m_{\bar{b}_j}^2, m_{\bar{b}_j}^2) - m_{\bar{g}}^2 D_2^e - s D_{12}^e - m_{\bar{t}_i}^2 D_{22}^e)] \}, \\
f_9^{\text{Box}(e)} &= \frac{2}{3} R_{j1}^{\bar{b}} \{ l_{jk}^{\bar{b}} [(m_{\bar{g}} R_{i1}^{\bar{t}} - m_t R_{i2}^{\bar{t}}) (D_{11}^e + 2D_{12}^e + D_{13}^e + D_1^e + D_{22}^e + D_{23}^e + D_2^e) \\
& + m_{\bar{g}} R_{i1}^{\bar{t}} (D_0^e + D_1^e + D_2^e + D_3^e)] - k_{jk}^{\bar{b}} m_{\bar{\chi}_k^-} R_{i2}^{\bar{t}} (D_{11}^e + D_{12}^e + D_{13}^e + D_1^e) \}, \\
f_{11}^{\text{Box}(e)} &= \frac{2}{3} R_{j1}^{\bar{b}} \{ l_{jk}^{\bar{b}} [m_t R_{i2}^{\bar{t}} (D_{12}^e + D_{22}^e) - m_{\bar{g}} R_{i1}^{\bar{t}} (D_{12}^e + D_{22}^e + D_2^e)] + k_{jk}^{\bar{b}} m_{\bar{\chi}_k^-} R_{i2}^{\bar{t}} D_{12}^e \}.
\end{aligned}$$

For the box diagram (f) in Fig.3, we find

$$\begin{aligned}
f_1^{\text{Box}(f)} &= \frac{1}{3} R_{j1}^{\bar{b}} \{ l_{jk}^{\bar{b}} [(m_t R_{i2}^{\bar{t}} - m_{\bar{g}} R_{i1}^{\bar{t}}) (C_0^k - 2D_{00}^f + s(D_0^f + D_1^f + D_2^f + D_3^f)) - m_t R_{i2}^{\bar{t}} (C_0^i \\
& + sD_0^f + t_1 D_0^f)] + k_{jk}^{\bar{b}} m_{\bar{\chi}_k^-} R_{i2}^{\bar{t}} [C_0^k + C_1(t, 0, m_{\bar{\chi}_k^-}^2; m_t^2, m_{\bar{g}}^2, m_{\bar{b}_j}^2) + C_2^i - 2D_{00}^f + sD_2^f \\
& - t_1(D_0^f + D_1^f + D_3^f)] \}, \\
f_3^{\text{Box}(f)} &= \frac{1}{3} R_{j1}^{\bar{b}} \{ l_{jk}^{\bar{b}} m_{\bar{\chi}_k^-} [m_{\bar{g}} R_{i1}^{\bar{t}} (D_0^f + D_1^f + D_3^f) - m_t R_{i2}^{\bar{t}} (D_1^f + D_3^f)] + k_{jk}^{\bar{b}} [R_{i2}^{\bar{t}} (C_0^i - C_0^k \\
& - C_0(0, m_{\bar{\chi}_k^-}^2, u; m_t^2, m_{\bar{t}}^2, m_{\bar{b}_j}^2) + 2D_{00}^f - m_{\bar{g}}^2 D_0^f - sD_2^f + t_1(D_0^f + D_3^f) - m_{\bar{t}_i}^2 (D_1^f + D_3^f)) \\
& + m_{\bar{g}} m_t R_{i1}^{\bar{t}} D_0^f] \}, \\
f_5^{\text{Box}(f)} &= \frac{2}{3} R_{j1}^{\bar{b}} \{ l_{jk}^{\bar{b}} m_{\bar{\chi}_k^-} [(m_t R_{i2}^{\bar{t}} - m_{\bar{g}} R_{i1}^{\bar{t}}) (D_{11}^f + D_{12}^f + 2D_{13}^f + D_1^f + D_{23}^f + D_{33}^f + D_3^f) \\
& - m_{\bar{g}} R_{i1}^{\bar{t}} (D_0^f + D_1^f + D_2^f + D_3^f)] - k_{jk}^{\bar{b}} [m_{\bar{g}} (m_t R_{i1}^{\bar{t}} - m_{\bar{g}} R_{i2}^{\bar{t}}) (D_0^f + D_1^f + D_2^f + D_3^f) \\
& + R_{i2}^{\bar{t}} (C_0^i + C_1^i + C_1(t, 0, m_{\bar{\chi}_k^-}^2; m_t^2, m_{\bar{g}}^2, m_{\bar{b}_j}^2) + C_2^i - 2D_{00}^f + (s - m_{\bar{t}_i}^2) (D_{11}^f + D_{12}^f \\
& + D_{13}^f + D_1^f) - m_{\bar{t}_i}^2 (D_{13}^f + D_{23}^f + D_{33}^f + D_3^f))] \}, \\
f_7^{\text{Box}(f)} &= \frac{2}{3} R_{j1}^{\bar{b}} \{ l_{jk}^{\bar{b}} m_{\bar{\chi}_k^-} [m_{\bar{g}} R_{i1}^{\bar{t}} (D_0^f + D_1^f + D_3^f) + (m_{\bar{g}} R_{i1}^{\bar{t}} - m_t R_{i2}^{\bar{t}}) (D_{11}^f + 2D_{13}^f \\
& + D_1^f + D_{33}^f + D_3^f)] + k_{jk}^{\bar{b}} [(m_{\bar{g}} m_t R_{i1}^{\bar{t}} - R_{i2}^{\bar{t}} (m_{\bar{g}}^2 - t_1)) (D_0^f + D_1^f + D_3^f) \\
& - R_{i2}^{\bar{t}} (\frac{1}{u_2} (B_0(m_{\bar{\chi}_k^-}^2, m_t^2, m_{\bar{b}_j}^2) - B_0(u, m_{\bar{t}}^2, m_{\bar{b}_j}^2)) - C_0^i + C_0^k - C_1^i - s(D_{11}^f + D_{13}^f \\
& + D_1^f - D_2^f) + m_{\bar{t}_i}^2 (D_{11}^f + 2D_{13}^f + D_1^f + D_{33}^f + D_3^f))] \}, \\
f_9^{\text{Box}(f)} &= \frac{2}{3} R_{j1}^{\bar{b}} \{ l_{jk}^{\bar{b}} [m_{\bar{g}} R_{i1}^{\bar{t}} (D_0^f + D_1^f + D_2^f + D_3^f) + (m_{\bar{g}} R_{i1}^{\bar{t}} - m_t R_{i2}^{\bar{t}}) (D_{13}^f + D_{23}^f + D_{33}^f \\
& + D_3^f)] + k_{jk}^{\bar{b}} m_{\bar{\chi}_k^-} R_{i2}^{\bar{t}} (D_{11}^f + D_{12}^f + D_{13}^f + D_1^f) \}, \\
f_{11}^{\text{Box}(f)} &= \frac{2}{3} R_{j1}^{\bar{b}} \{ l_{jk}^{\bar{b}} [m_t R_{i2}^{\bar{t}} (D_{13}^f - D_1^f + D_{33}^f) - m_{\bar{g}} R_{i1}^{\bar{t}} (D_{13}^f + D_{33}^f + D_3^f)] \\
& - k_{jk}^{\bar{b}} m_{\bar{\chi}_k^-} R_{i2}^{\bar{t}} (D_{11}^f + D_{13}^f + D_1^f) \}.
\end{aligned}$$

For the box diagram (g) in Fig.3, we find

$$f_1^{\text{Box}(g)} = \frac{7}{6t_2} l_{ik}^{\bar{t}} m_{\bar{\chi}_k} (B_0(m_{\bar{\chi}_k}^2, 0, m_{\bar{t}_i}^2) - B_0(t, 0, m_{\bar{t}_i}^2)),$$

$$f_5^{\text{Box}(g)} = -\frac{7}{3} l_{ik}^{\bar{t}} C_2^e.$$

APPENDIX B

In this Appendix, we collect the explicit expressions for the amplitudes squared of the radiations of a real gluon and a massless (anti-)quark. Since these expressions are only used to the hard non-collinear parts of real corrections in Eq.(3.16) and Eq.(3.35), they have no singularities and can be calculated in $n = 4$ dimensions.

For the real gluon emission, we find

$$\overline{|M_{ik}^{gb}|^2} = X_{ik} [\overline{|M^{(s)}|^2} + \overline{|M^{(t)}|^2} + \overline{|M^{(st)}|^2}] + (s \leftrightarrow t', s_4 \leftrightarrow u_7, s_{3\Delta} \leftrightarrow u_2),$$

where $X_{ik} = g^2 g_s^4 (|l_{ik}^{\bar{t}}|^2 + |k_{ik}^{\bar{t}}|^2)$, and

$$\begin{aligned} \overline{|M^{(s)}|^2} &= \frac{1}{s s_5} \left\{ \frac{1}{36 s_4 t'} [t_2 u' m_{\bar{t}_i}^2 - s_4 u_6 (t_2 + u_2) + u_6 (u_6 (s_{3\Delta} - u_2) + (s_5 + u_7) (s_{3\Delta} + t_2) \right. \\ &\quad \left. - u' (s_{5\Delta} + m_{\bar{\chi}_k}^2)) - s_4 t' m_{\bar{\chi}_k}^2] - \frac{1}{8 s_4 u'} [s_{5\Delta} t' u_6 + u_6^2 (u_2 - s_{3\Delta}) - u_6 u_7 (s_{3\Delta} + t_2 \right. \\ &\quad \left. + u_2) + (s_4 t_2 - s s_{5\Delta}) (u_6 + u_7) + t_2 u_7^2 - m_{\bar{t}_i}^2 (u_2 (2s + t') + 4t_2 t' - 3s s_{3\Delta}) \right. \\ &\quad \left. - m_{\bar{\chi}_k}^2 (2u_6 (t' + s) + u_7 (4s + t'))] - \frac{t'}{8 s_5 u'} [\Delta_t (4t_2 + u_2) + (4u_6 + u_7) (2m_{\bar{\chi}_k}^2 + s_{5\Delta})] \right. \\ &\quad \left. - \frac{u'}{36 s_5 t'} [\Delta_t t_2 + u_6 (s_{5\Delta} + 2m_{\bar{\chi}_k}^2)] - \frac{1}{72 s_4} [11 s_{5\Delta} u_6 - m_{\bar{t}_i}^2 (31t_2 + 34u_2) - m_{\bar{\chi}_k}^2 (9u_6 \right. \\ &\quad \left. + 34u_7)] - \frac{1}{72 s_5} [\Delta_t (31t_2 + 16u_2) + (31u_6 + 16u_7) (s_{5\Delta} + 2m_{\bar{\chi}_k}^2)] \right\} \\ &\quad + \frac{1}{s_5^2} \left\{ \frac{1}{8 u'^2} [4s (\Delta_t s_{3\Delta} + s_4 s_{5\Delta} + 2s_4 m_{\bar{\chi}_k}^2) + u' \Delta_t (u_2 - 2t_2) + u' (s_4 - 2u_6) (s_{5\Delta} \right. \\ &\quad \left. + 2m_{\bar{\chi}_k}^2) + s_5 u' (s_{5\Delta} - m_{\bar{\chi}_k}^2)] \right\} + \frac{4u_2}{9 s s_4^2} m_{\bar{t}_i}^2, \\ \overline{|M^{(t)}|^2} &= \frac{1}{t_1^2} \left\{ \frac{1}{16 u'^2} [2t_2 (s_{3\Delta} - s_4 + t') (s + u_2 - u_7) + 4t_2 u' (s_4 + s_{5\Delta} + u_6 - m_{\bar{t}_i}^2) + s_{5\Delta} t_1 u'] \right. \\ &\quad \left. - \frac{t_2}{4 s_4 u'} [u_7 (s_{3\Delta} + s_{5\Delta} + t' + u_6) - m_{\bar{t}_i}^2 (s - s_{3\Delta} - t' + u_2 + u_7)] + \frac{1}{36 s_4 u_7} [t_2 (4m_{\bar{\chi}_k}^4 \right. \\ &\quad \left. + s_4 u_7) + 2s_{5\Delta} t_1 m_{\bar{t}_i}^2] - \frac{1}{18 s_4^2} [m_{\bar{t}_i}^2 (t_2 (16m_{\bar{t}_i}^2 + 7s_4) + 8t_1 (s_{3\Delta} + s_{5\Delta})) - \frac{9}{4} s_4 s_{5\Delta} t_1] \right\} \\ &\quad - \frac{1}{16 s_4 t_1 u'} [t_2 u_7 + 4s_{3\Delta} m_{\bar{t}_i}^2 + 4u_7 m_{\bar{\chi}_k}^2 - s_{5\Delta} (s + s_{3\Delta} - t' + u_2 + u_7) - u_6 (2s_{3\Delta} \end{aligned}$$

$$\begin{aligned}
& -2t_2 - u_2)], \\
\overline{|M^{(st)}|^2} &= \frac{1}{36s_5t_1} \left\{ \frac{9}{s_4u'} [u_7(s_{5\Delta}t' - s_{3\Delta}u_6 + 2m_{\tilde{\chi}_k^-}^2(t' + u_6)) + m_{\tilde{t}_i}^2(u_6(u_2 - s_{3\Delta}) + t_2u_7 \right. \\
& + (s_{5\Delta} + 2m_{\tilde{\chi}_k^-}^2)(t' - s))] + \frac{1}{2s_{S4}} [16m_{\tilde{t}_i}^2(u_2(t' + u_6) + t_2(2t' + 2u_6 + u_7 + u')) \\
& + 16m_{\tilde{\chi}_k^-}^2(t'(2u_6 + u_7) + u_6(2u_6 + 2u_7 + u')) - s_4t_2(9s_{5\Delta} + 2u_6 - 7u_7 - 7m_{\tilde{t}_i}^2) \\
& + 7s_4u_2u_6 + s_{S4}(7s_{5\Delta} - 2m_{\tilde{\chi}_k^-}^2) - (9s_5(s_{5\Delta}t_2 + 3t_2u_6 + u_2u_6 + t_2u_7) + 14s_5t_2m_{\tilde{t}_i}^2 \\
& + s_4m_{\tilde{\chi}_k^-}^2(9t_2 - 14u_6) - 2su_6(s_{5\Delta} + 2m_{\tilde{\chi}_k^-}^2) - 2sm_{\tilde{t}_i}^2(8s_{3\Delta} + 7s_{5\Delta} + 14m_{\tilde{\chi}_k^-}^2)] \\
& - \frac{9}{4su'} [2t'(\Delta_t + s_{5\Delta})(2t_2 + u_2) + (s_{3\Delta} - s_4 - 2t_2 - t' - u_2 + 2u_6 + u_7)(t_2u_7 \\
& - u_2u_6) + (s_5t_2 - 4t'm_{\tilde{\chi}_k^-}^2)(2u_6 + u_7) - 3ss_4t_2 - 2s\Delta_t(2t_2 + u_2) - 2ss_{5\Delta}(t_2 \\
& + u_2 - u_6) + 4sm_{\tilde{\chi}_k^-}^2(s_4 + 3u_6) + (s_5 - s)u_2u_6] - \frac{9}{u'^2} [ss_{5\Delta}(s_{3\Delta} - s_4 + t') + (s \\
& + u_2)(s_4t_2 + s_{3\Delta}u_6) + s_4(u_2u_6 - t_2u_7) + 2t'm_{\tilde{\chi}_k^-}^2(s + u_2 - u_7)] - \frac{1}{su_7} [t_1u_6(s_{5\Delta} \\
& + 2m_{\tilde{\chi}_k^-}^2) - u_6^2(u_2 - 2m_{\tilde{\chi}_k^-}^2) + t_1u_2m_{\tilde{t}_i}^2 + u_6m_{\tilde{t}_i}^2(2t_2 + u_2)] \left. \right\} + \frac{1}{36s_{S4}} \left\{ \frac{1}{2t'u_7} [2u_6^2(t_2 \right. \\
& + u_2) - s_{5\Delta}u_6u' + t_2u'm_{\tilde{t}_i}^2] - \frac{9}{4t_1u'} [(2t_2 + u_2)(u_6(t' - s_{3\Delta} + u_2 + u_7) + 2t'(s_{5\Delta} \\
& - 2m_{\tilde{t}_i}^2)) - t_2u_7(s_{3\Delta} + 4t_2 + t' + 3u_2 - u_7)] + \frac{16m_{\tilde{t}_i}^2}{s_4t_1} [u_2(t' + u_6) + t_2(2t' + 2u_6 \\
& + u_7 + u')] - \frac{1}{t_1u_7} [2u_6m_{\tilde{t}_i}^2(2t_2 + u_2) + t_1(s_{5\Delta}u_6 + u_2m_{\tilde{t}_i}^2)] \left. \right\}.
\end{aligned}$$

For the subprocess with two initial-state gluons, we find

$$\overline{|M_{ik}^{gg}|^2} = -\frac{3}{8} \overline{|M_{ik}^{gb}|^2} (s \leftrightarrow u', \quad s_4 \leftrightarrow u_6, \quad s_3 \rightarrow s_4 + u_7 + u', \quad s_{3\Delta} \rightarrow s_4 + u_7 + u' + \Delta_t).$$

For the subprocess with the initial-state $q\bar{q}$, we find

$$\begin{aligned}
\overline{|M_{ik}^{q\bar{q}}|^2} &= \frac{1}{9s^2} X_{ik} \left\{ \frac{2}{s_5^2} [\Delta_t(t'u_2 + t_2u') + (t'u_7 + u_6u')(s_{5\Delta} + 2m_{\tilde{\chi}_k^-}^2)] - \frac{1}{s_3^2} [ss_3(\Delta_s + s_3 \right. \\
& - s_4 - s_{5\Delta}) + s_3(t_2 + t' - u_6)(u_7 - u_2 - u')] - \frac{1}{s_3s_5} [s_{5\Delta}t'u_2 - 2ss_3(\Delta_t + s_{5\Delta}) \\
& - s_4u_2(2t_2 + t' - u_6) + t'u_7(s_3 - s_{5\Delta}) - s_3u_7(2u_6 - t_2) + s_3u_6(u_2 + u') - s_4t_2(u' \\
& - u_7) - 2m_{\tilde{\chi}_k^-}^2(t'(u_7 - u_2) - 2ss_4) + u'(t_2 + 2t' - u_6)(s_{5\Delta} + 2m_{\tilde{\chi}_k^-}^2)] \left. \right\}.
\end{aligned}$$

For the subprocess with the initial-state bq or $b\bar{q}$, we find

$$\overline{|M_{ik}^{bq(\bar{q})}|^2} = \overline{|M_{ik}^{q\bar{q}}|^2} (s \leftrightarrow u', \quad s_4 \leftrightarrow u_6, \quad t_2 \leftrightarrow s_{3\Delta}, \quad s_3 \rightarrow t_2, \quad \frac{1}{s_3} \rightarrow \frac{1}{t_1}).$$

For the subprocess with the initial-state $b\bar{b}$, we find

$$\begin{aligned}
\overline{|M_{ik}^{bb}|^2} &= \frac{1}{27} X_{ik} \left\{ \frac{3s_{3\Delta}}{s^2 s_3^2} [s(s_4 + s_{5\Delta} - \Delta_s - s_{3\Delta}) + (t_2 + t' - u_6)(u_2 - u_7 + u')] \right. \\
&\quad + \frac{2t'}{s s_5^2 u'} [s_{5\Delta} u_7 - u_2 m_{\tilde{t}_i}^2 + (u_2 + 2u_7) m_{\tilde{\chi}_k^-}^2] - \frac{1}{s s_3 s_5 u'} [\Delta_s t' u_2 - s s_{3\Delta} s_{5\Delta} \\
&\quad + s_{3\Delta} u_6 (u_2 - u_7) + s_4 t_2 u_7 + (s_{3\Delta} - s_{5\Delta}) t' u_7 + (t_2 + t') (-s_4 u_2 + s_{5\Delta} u') \\
&\quad - \Delta_t (s s_{3\Delta} - t_2 u') + 2(ss_4 + (t' - u_6) u') m_{\tilde{\chi}_k^-}^2] + \frac{1}{4 s s_3 t_1 u'} [2 s s_{3\Delta} (s_{3\Delta} - s_4 \\
&\quad - s_{5\Delta} + t') - t' u_2 (2t_2 - 2s_4 + t') + m_{\tilde{\chi}_k^-}^2 (2t_2 u' + t' (u_2 - 2u_7 + 4u_p)) + 2(s_4 t_2 \\
&\quad - s_{3\Delta} t_2) (s + u_2 - u_7) + s_{5\Delta} t' (u_7 - 2s) + m_{\tilde{t}_i}^2 (2t_2 u' - t' u_2)] + \frac{6}{s^2 s_5^2} [\Delta_t (t' u_2 + t_2 u') \\
&\quad + (t' u_7 + u_6 u') (s_{5\Delta} + 2m_{\tilde{\chi}_k^-}^2)] - \frac{3}{s^2 s_3 s_5} [s_{5\Delta} t' (u_2 - u_7) - 2 s s_{3\Delta} (\Delta_t + s_{5\Delta}) \\
&\quad - s_4 u_2 (2t_2 + t') + s_{3\Delta} u_7 (t' - 2u_6) + (s_{3\Delta} + s_4) (u_2 u_6 + t_2 u_7) - s_4 t_2 u' + s_{5\Delta} u' (t_2 \\
&\quad + 2t' - u_6) + s_{3\Delta} u_6 u' + 2m_{\tilde{\chi}_k^-}^2 (2ss_4 + (t_2 + 2t' - u_6) u' + t' (u_2 - u_7))] \left. \right\} \\
&\quad + (s \leftrightarrow u', \quad s_4 \leftrightarrow u_6, \quad t_2 \leftrightarrow s_{3\Delta}, \quad s_3 \leftrightarrow t_1).
\end{aligned}$$

For the subprocess with the initial-state $b\bar{b}$, we find

$$\overline{|M_{ik}^{bb}|^2} = \overline{|M_{ik}^{bb}|^2} (s \leftrightarrow t', \quad s_4 \leftrightarrow u_7, \quad u_2 \leftrightarrow s_{3\Delta}, \quad s_3 \leftrightarrow u_1).$$

-
- [1] F. Gianotti, M.L. Mangano, T. Virdee, hep-ph/0204087.
- [2] H.P. Nilles, Phys. Rep. 110 (1984) 1; H.E. Haber and G.L. Kane, Phys. Rep. 117 (1985) 75; A.B. Lahanas, D.V. Nanopoulos, Phys. Rep. 145 (1987) 1; Supersymmetry, Vols. 1 and 2, ed. S. Ferrara (North Holland/World Scientific, Singapore, 1987). For a recent review, consult S. Dawson, TASI-97 lectures, hep-ph/9712464.
- [3] G.L. Kane and J.P. Leveille, Phys. Lett. B 112 (1982) 227; P.R. Harrison and C.H. Llewellyn Smith, Nucl. Phys. B 213 (1983) 223; Nucl. Phys. B 223 (1983) 542 (E); E. Reya and D.P. Roy, Phys. Rev. D 32 (1985) 645; S. Dawson, E. Eichten, C. Quigg, Phys. Rev. D 31 (1985) 1581; H. Baer and X. Tata, Phys. Lett. B 160 (1985) 159.
- [4] W. Beenakker, R. Höpker, M. Spira, P.M. Zerwas, Nucl. Phys. B 492 (1997) 51.
- [5] W. Beenakker, R. Höpker, M. Spira, P.M. Zerwas, Phys. Rev. Lett. 74 (1995) 2905; Z. Phys. C 69 (1995) 163.

- [6] W. Beenakker, M. Krämer, T. Plehn, P.M. Zerwas, Nucl. Phys. B 515 (1998) 3.
- [7] W. Beenakker, M. Klasen, M. Krämer, T. Plehn, M. Spira, P.M. Zerwas, Phys. Rev. Lett. 83 (1999) 3780.
- [8] H. Baer, B.W. Harris, M.H. Reno, Phys. Rev. D 57 (1998) 5871.
- [9] E.L. Berger, M. Klasen, T.M.P. Tait, Phys. Lett. B 459 (1999) 165; Phys. Rev. D 62 (2000) 095014; hep-ph/0212306 (E).
- [10] J.F. Gunion, H.E. Haber, F.E. Paige, W.-K. Tung, S. Willenbrock, Nucl. Phys. B 294 (1987) 621; R.M. Barnett, H.E. Haber, D.E. Soper, Nucl. Phys. B 306 (1988) 697; F.I. Olness and W.-K. Tung, Nucl. Phys. B 308 (1988) 813; V. Barger, R.J.N. Phillips, D.P. Roy, Phys. Lett. B 324 (1994) 236; C.S. Huang and S.H. Zhu, Phys. Rev. D 60 (1999) 075012; L.G. Jin, C.S. Li, R.J. Oakes, S.H. Zhu, Phys. Rev. D 62 (2000) 053008; S.H. Zhu, hep-ph/0112109.
- [11] M. A. Aivazis, J. C. Collins, F. I. Olness, and W. K. Tung, Phys. Rev. D 50 (1994) 3102; J. C. Collins, Phys. Rev. D 58 (1998) 094002; M. Krämer, F. I. Olness, D. E. Soper, Phys. Rev. D 62 (2000) 096007.
- [12] D. Cavalli, *et al.*, 'The Higgs working group: Summary Report', Los Houches 2001, "Physics at TeV Colliders", hep-ph/0203056; D. Rainwater, M. Spira, D. Zeppenfeld, hep-ph/0203187; M. Spira, hep-ph/0211145.
- [13] D.A. Dicus, T. Stelzer, Z. Sullivan, S. Willenbrock, Phys. Rev. D 59 (1999) 094016; C. Balazs, H.-J. He, C.P. Yuan, Phys. Rev. D 60 (1999) 114001.
- [14] J. Campbell, R.K. Ellis, F. Maltoni, S. Willenbrock, hep-ph/0204093.
- [15] T. Plehn, hep-ph/0206121; F. Maltoni, Z. Sullivan, S. Willenbrock, hep-ph/0301033.
- [16] J.F. Gunion and H. Haber, Nucl. Phys. B 272 (1986) 1.
- [17] W. Beenakker, R. Höpker, P.M. Zerwas, Phys. Lett. B 378 (1996) 159; W. Beenakker, R. Höpker, T. Plehn, P.M. Zerwas, Z. Phys. C 75 (1997) 349.
- [18] M. Chanowitz, M. Furman, I. Hinchliffe, Nucl. Phys. B 159 (1979) 225.
- [19] A. Sirlin, Phys. Rev. D 22 (1980) 971; W. J. Marciano and A. Sirlin, Phys. Rev. D 22 (1980) 2695; Phys. Rev. D 31 (1985) 213 (E); A. Sirlin and W.J. Marciano, Nucl. Phys. B 189 (1981) 442; K.I. Aoki et.al., Prog. Theor. Phys. Suppl. 73 (1982) 1.
- [20] A. Denner, Fortschr. Phys. 41 (1993) 4.
- [21] J. Guasch, W. Hollik, J. Solà, Phys. Lett. B 437 (1998) 88.
- [22] J. Collins, F. Wilczek, A. Zee, Phys. Rev. D 18 (1978) 242; W. J. Marciano, Phys. Rev. D 29

- (1984) 580; Phys. Rev. D 31 (1984) 213 (E); P. Nason, S. Dawson, R.K. Ellis, Nucl. Phys. B 327 (1989) 49; Nucl. Phys. B 335 (1989) 260 (E).
- [23] G. Altarelli, R.K. Ellis, G. Martinelli, Nucl. Phys. B 157 (1979) 461; J.C. Collins, D.E. Soper, G. Sterman, in: Perturbative Quantum Chromodynamics, ed. A.H. Mueller (World Scientific, 1989).
- [24] W. Beenakker, H. Kuijf, W.L. van Neerven, and J. Smith, Phys. Rev. D 40 (1989) 54.
- [25] B.W. Harris and J.F. Owens, Phys. Rev. D 65 (2002) 094032.
- [26] G.P. Lepage, J. Comp. Phys. 27 (1978) 192.
- [27] J.C. Collins, D.E. Soper, and G. Sterman, Nucl. Phys. B 261 (1985) 104; G.T. Bodwin, Phys. Rev. D 31 (1985) 2616; Phys. Rev. D 34 (1986) 3932 (E).
- [28] G. Altarelli and G. Parisi, Nucl. Phys. B 126 (1977) 298.
- [29] R. K. Ellis, D.A. Ross, and A.E. Terrano, Nucl. Phys. B 178 (1981) 421; L.J. Bergmann, in: Next-to-leading-log QCD calculation of symmetric dihadron production (Ph.D. thesis, Florida State University, 1989); Z. Kunszt and D.E. Soper, Phys. Rev. D 46 (1992) 192; M.L. Mangano, P. Nason, G. Ridolfi, Nucl. Phys. B 373 (1992) 295.
- [30] Particle Data Group, K. Hagiwara, et al, Phys. Rev. D 66 (2002) 1.
- [31] S.G. Gorishny, A.L. Kataev, S.A. Larin, L.R. Surguladze, Mod. Phys. Lett. A 5 (1990) 2703; Phys. Rev. D 43 (1991) 1633; A. Djouadi, M. Spira, P.M. Zerwas, Z. Phys. C 70 (1996) 427; A. Djouadi, J. Kalinowski, M. Spira, Comput. Phys. Commun. 108 (1998) 56; M. Spira, Fortschr. Phys. 46 (1998) 203.
- [32] J. Pumplin, D.R. Stump, J. Huston, H.L. Lai, P. Nadolsky, W.K. Tung, hep-ph/0201195.
- [33] M. Carena, D. Garcia, U. Nierste, C.E.M. Wagner, Nucl. Phys. B 577 (2000) 88.
- [34] M. Beneke and A. Signer, Phys. Lett. B 471 (1999) 233; A.H. Hoang, Phys. Rev. D 61 (2000) 034005.
- [35] K. Hidaka and A. Bartl, Phys. Lett. B 501 (2001) 78.
- [36] H. Eberl, K. Hidaka, S. Kraml, W. Majerotto, and Y. Yamada, Phys. Rev. D 62 (2000) 055006; A. Savoy-Navarro, talk at the International Europhysics Conference on High Energy Physics (HEP99), 1999, Tampere, Finland. For transparencies see [Http://neutrino.pc.helsinki.fi/hep99/Transparencies/session-07/Savoy-Navarro.pdf](http://neutrino.pc.helsinki.fi/hep99/Transparencies/session-07/Savoy-Navarro.pdf).

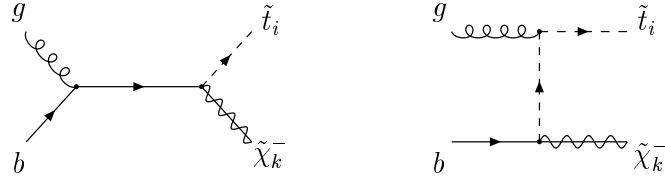


FIG. 1: Leading order feynman diagrams for $gb \rightarrow \tilde{t}_i \tilde{\chi}_k^-$.

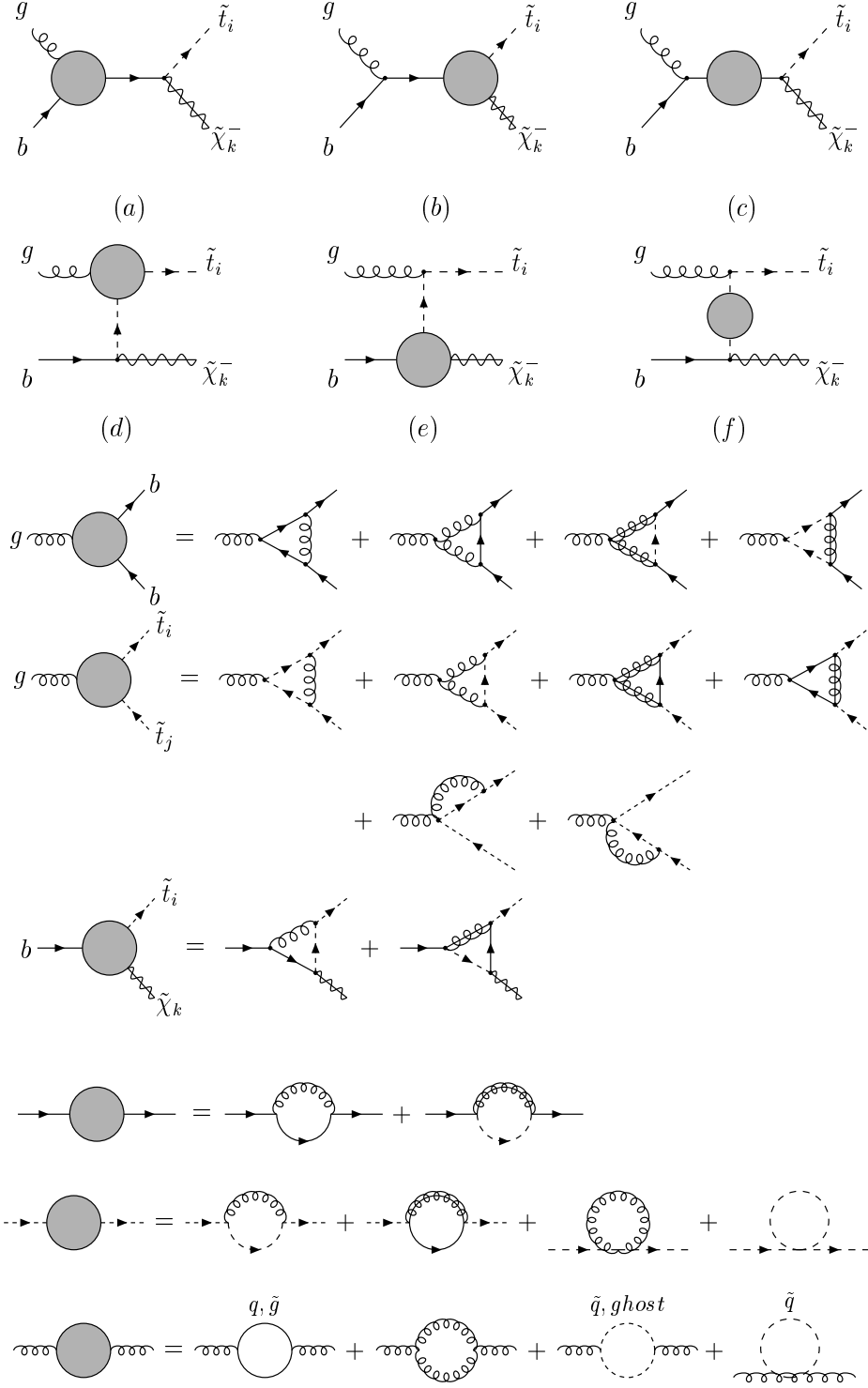


FIG. 2: Virtual one-loop Feynman diagrams including self-energy and vertex corrections for $gb \rightarrow \tilde{t}_i \tilde{\chi}_k^-$.

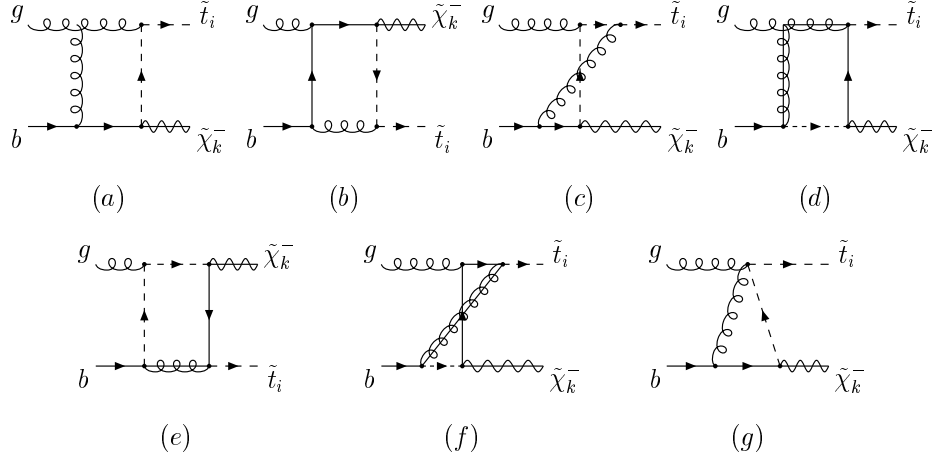


FIG. 3: Box Feynman diagrams for $gb \rightarrow \tilde{t}_i \tilde{\chi}_k^-$.

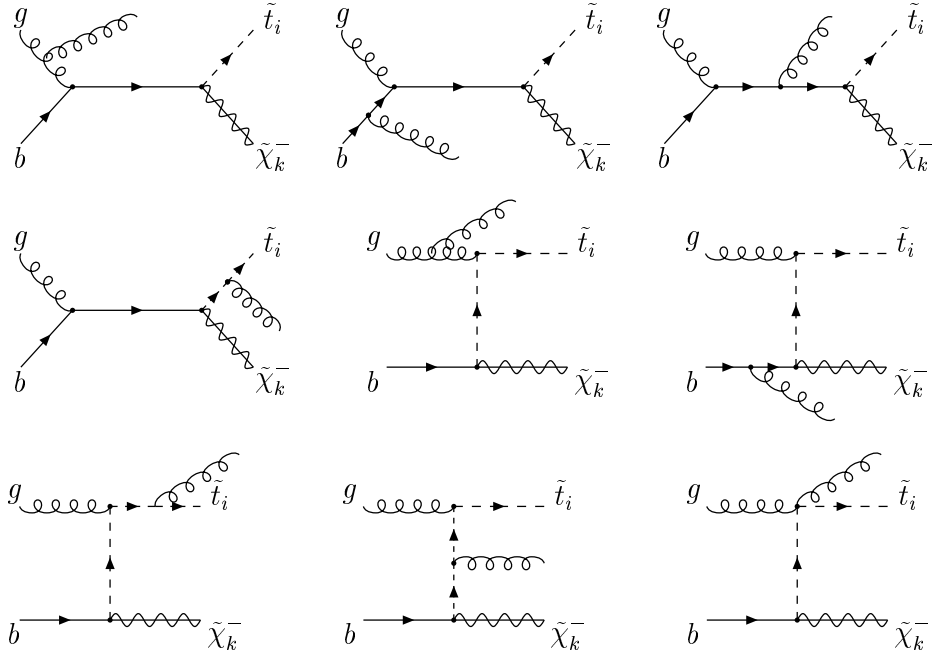


FIG. 4: Feynman diagrams for the real gluon emission contributions.

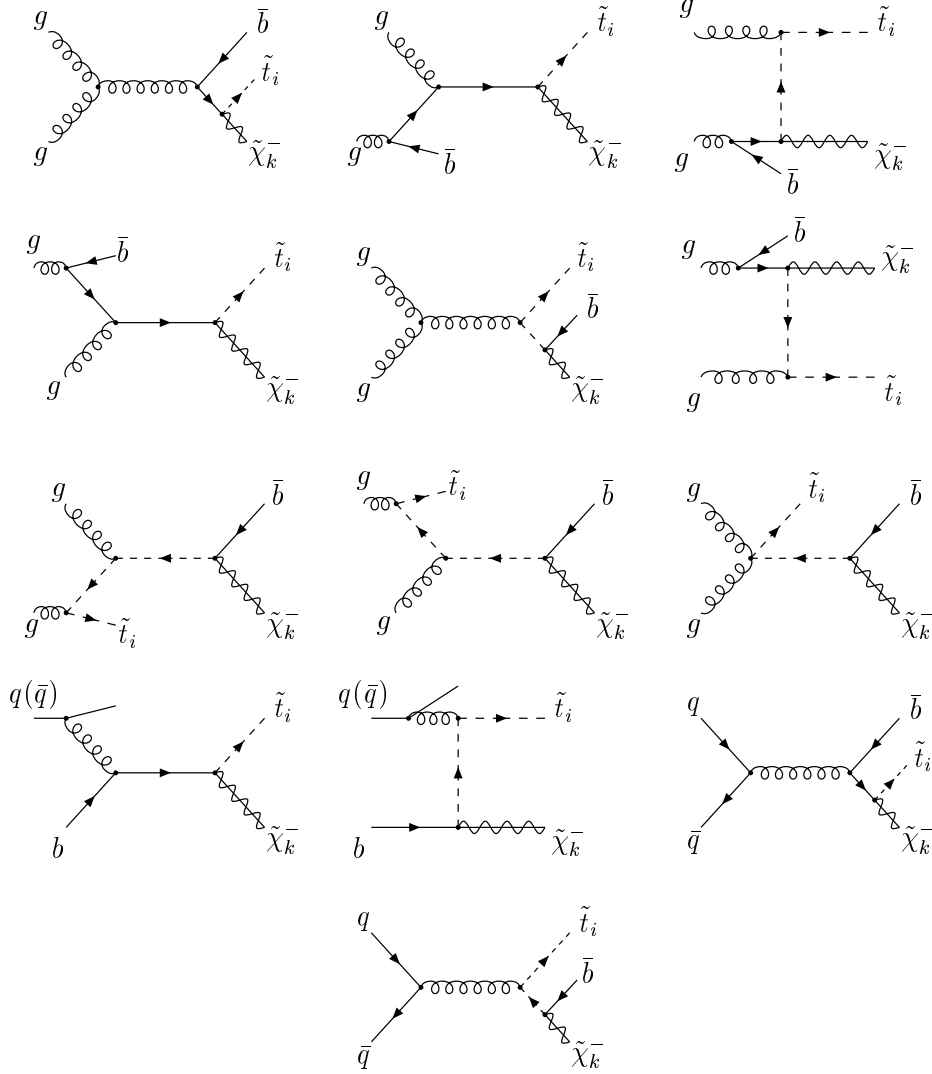


FIG. 5: Feynman diagrams for the emission of a massless (anti)quark. Here $q = u, d, c, s, b$.

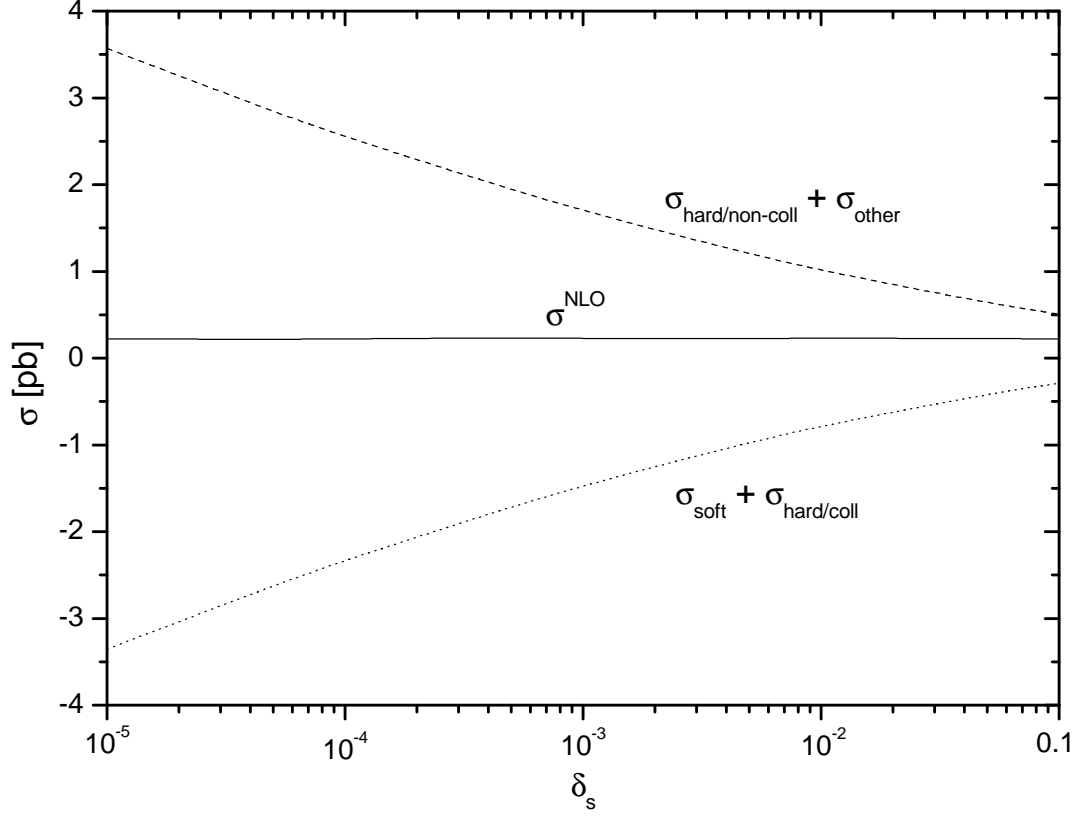


FIG. 6: Dependence of the total cross sections for the $\tilde{t}_1\tilde{\chi}_1^-$ production at the LHC on the cutoff δ_s , assuming $\mu = -200$ GeV, $M_2 = 300$ GeV, $m_{\tilde{t}_1} = 250$ GeV, $\tan\beta = 30$ and $\delta_c = \delta_s/100$.

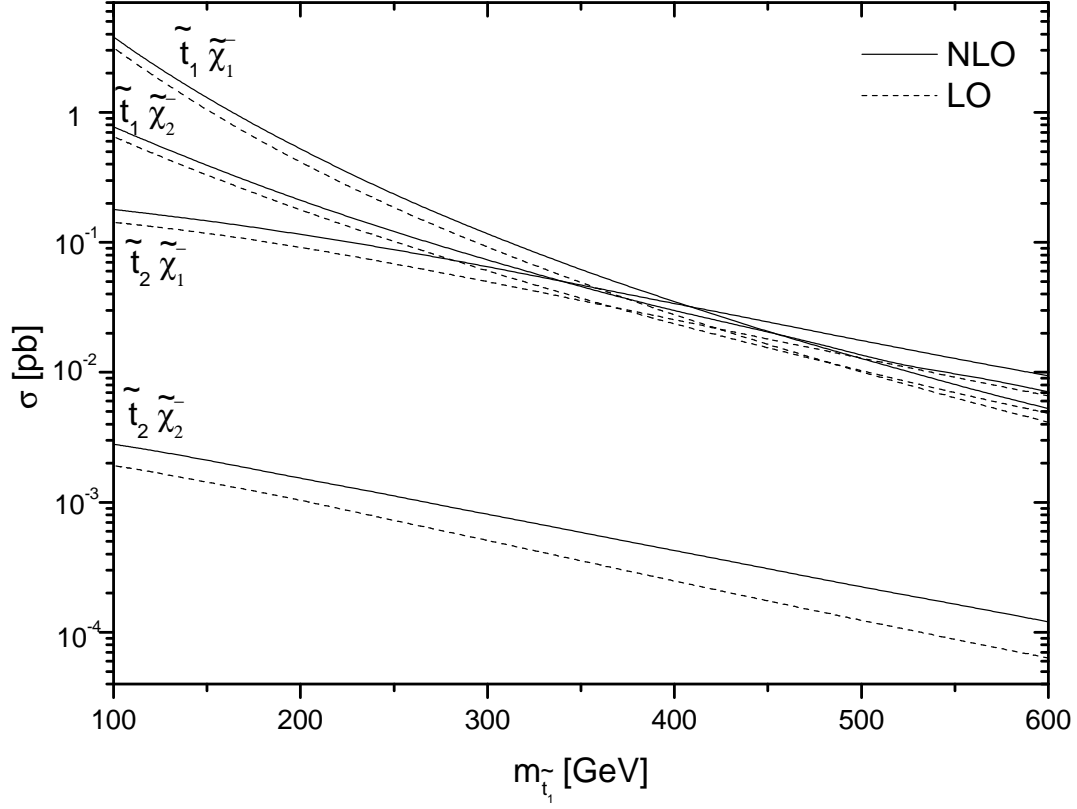


FIG. 7: Dependence of the total cross sections on $m_{\tilde{t}_1}$ for the $\tilde{t}_i \tilde{\chi}_k^-$ productions at the LHC, assuming $\mu = -200$ GeV, $M_2 = 300$ GeV and $\tan \beta = 30$.

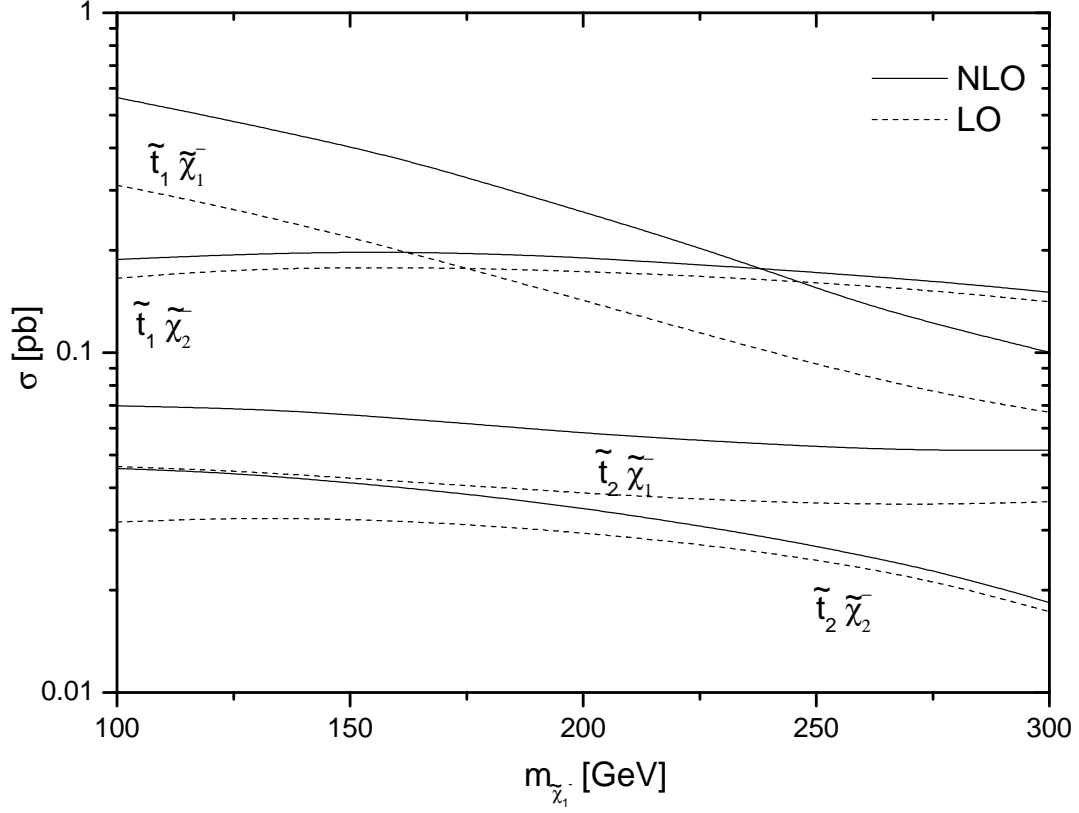


FIG. 8: Dependence of the total cross sections on $m_{\tilde{\chi}_1^-}$ for the $\tilde{t}_i\tilde{\chi}_k^-$ productions at the LHC, assuming $\mu = -400$ GeV, $m_{\tilde{t}_1} = 250$ GeV and $\tan\beta = 30$.

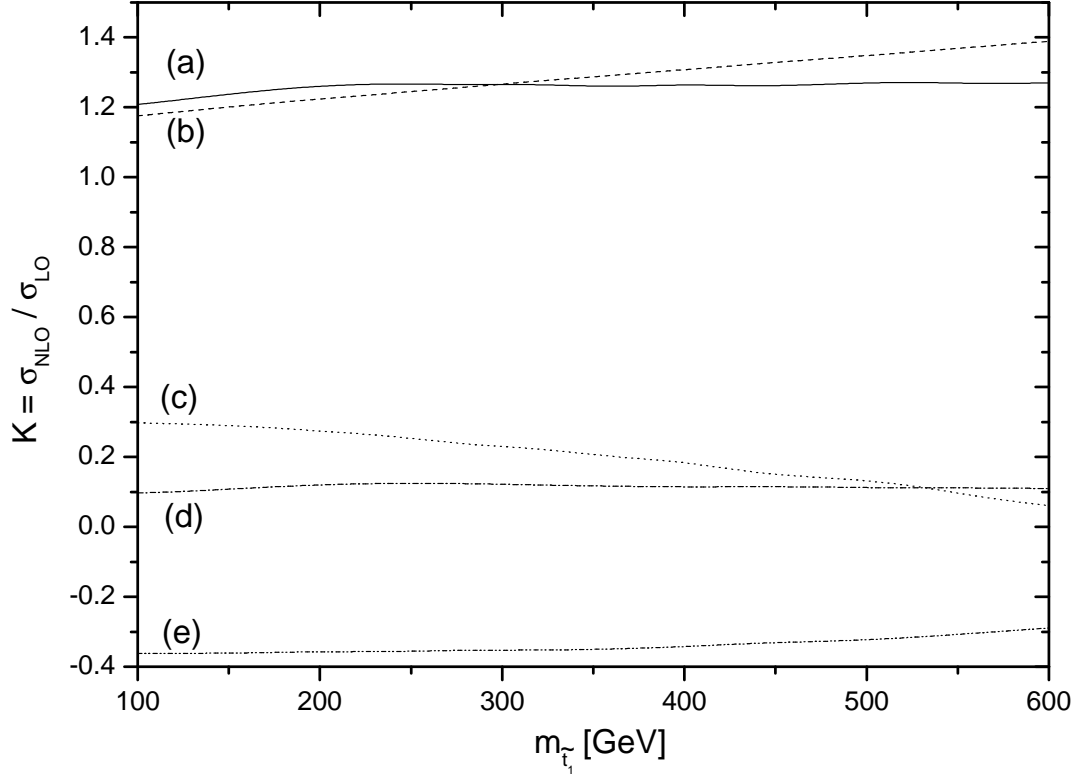


FIG. 9: $K = \sigma_{NLO}/\sigma_{LO}$ factor for the $\tilde{t}_1\tilde{\chi}_1^-$ production at the LHC as a function of $m_{\tilde{t}_1}$, assuming $\mu = -200$ GeV, $M_2 = 300$ GeV and $\tan\beta = 30$. σ_{NLO} is the NLO total cross section for (a), the improved Born cross section for (b), the corrections of the subprocess with two initial-state gluons for (c), the corrections of the massless (anti)quark emission subprocess Eq.(3.30)-(3.32) for (d), and the virtual and real gluon emission corrections for (e).

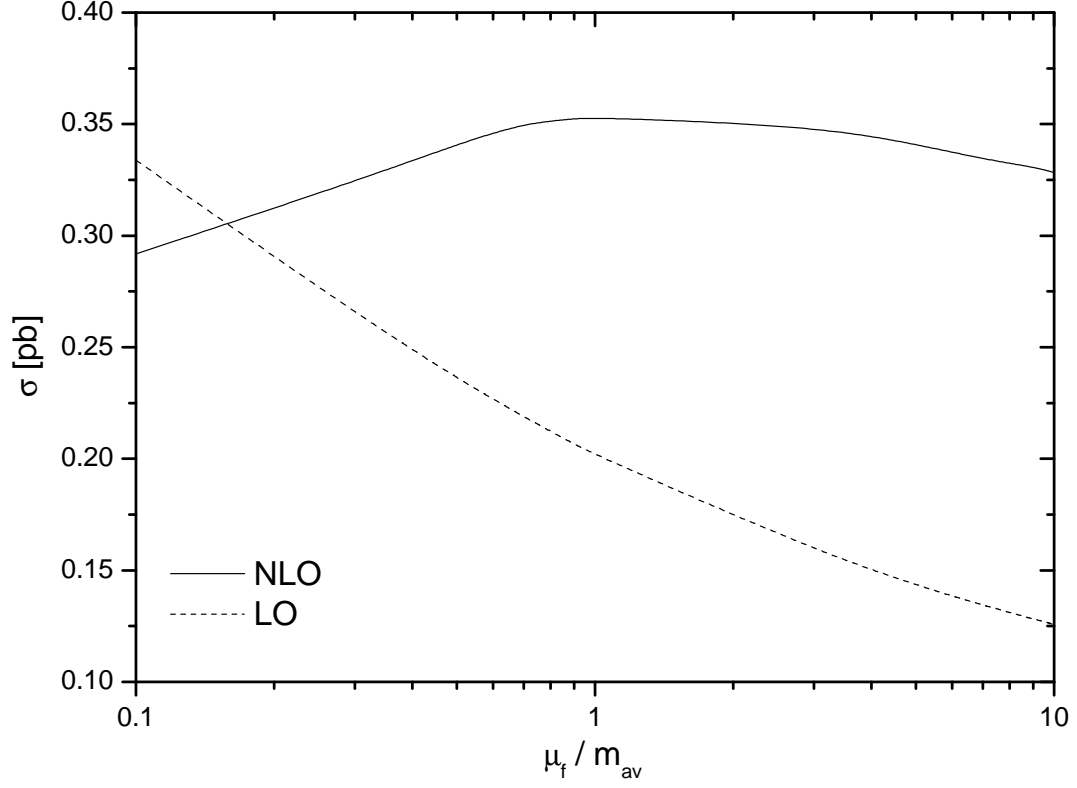


FIG. 10: Dependence of the total cross sections for the $\tilde{t}_1\tilde{\chi}_1^-$ production at the LHC on the renormalization/factorization scale, assuming $\mu = -200$ GeV, $M_2 = 300$ GeV, $\tan\beta = 30$, $m_{\tilde{t}_1} = 250$ GeV, $\mu_r = \mu_f$ and $m_{av} = (m_{\tilde{t}_1} + m_{\tilde{\chi}_1^-})/2$.

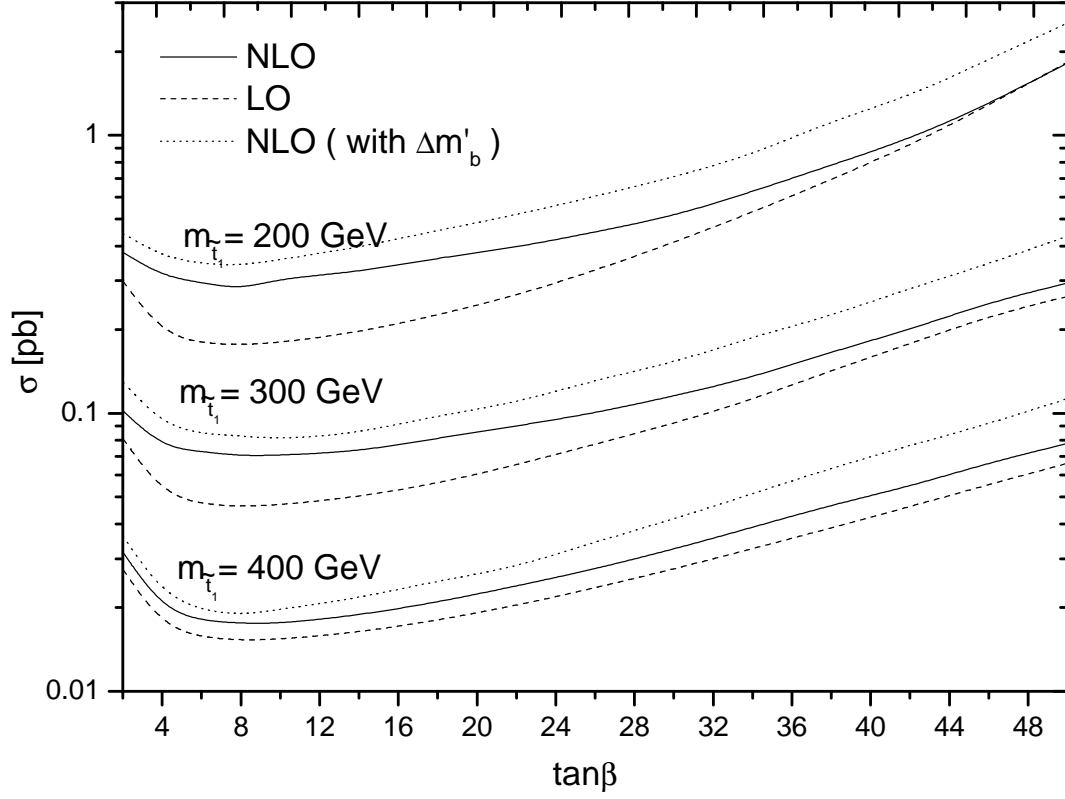


FIG. 11: Dependence of the total cross sections for the $\tilde{t}_1 \tilde{\chi}_1^-$ production at the LHC on the parameter $\tan\beta$, assuming $\mu = -200$ GeV and $M_2 = 300$ GeV.

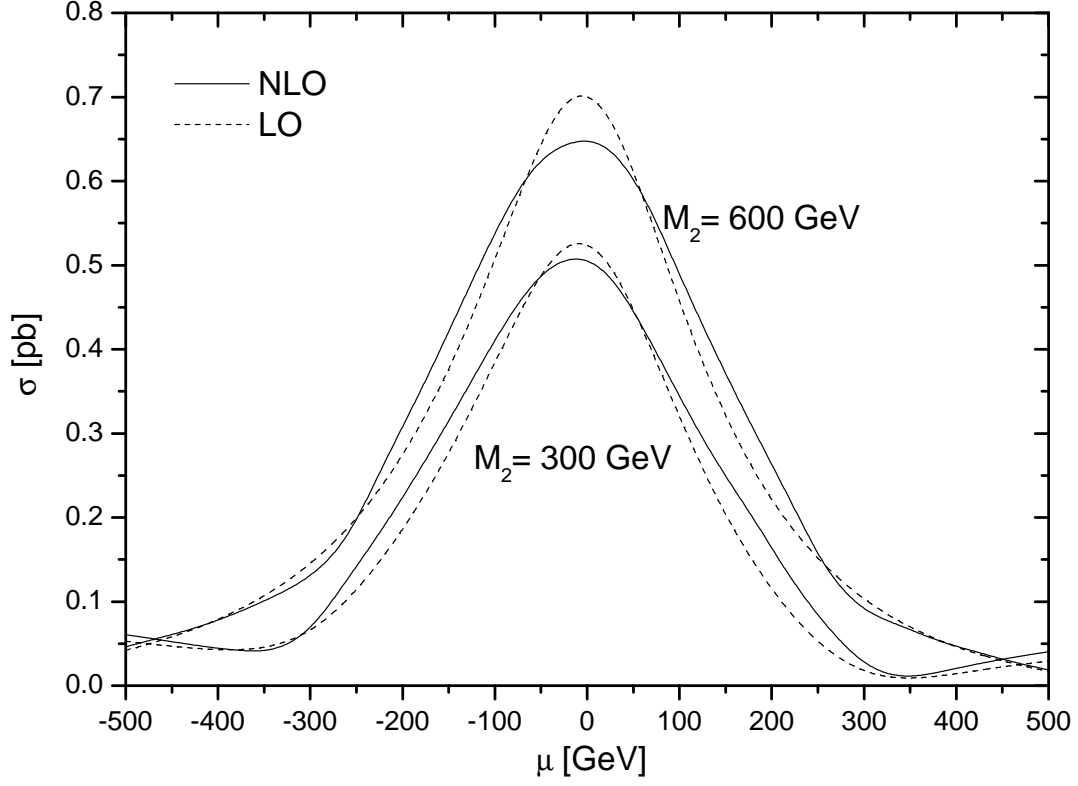


FIG. 12: Dependence of the total cross sections for the $\tilde{t}_1\tilde{\chi}_1^-$ production at the LHC on the parameter μ , assuming $m_{\tilde{t}_1} = 250$ GeV and $\tan\beta = 30$.

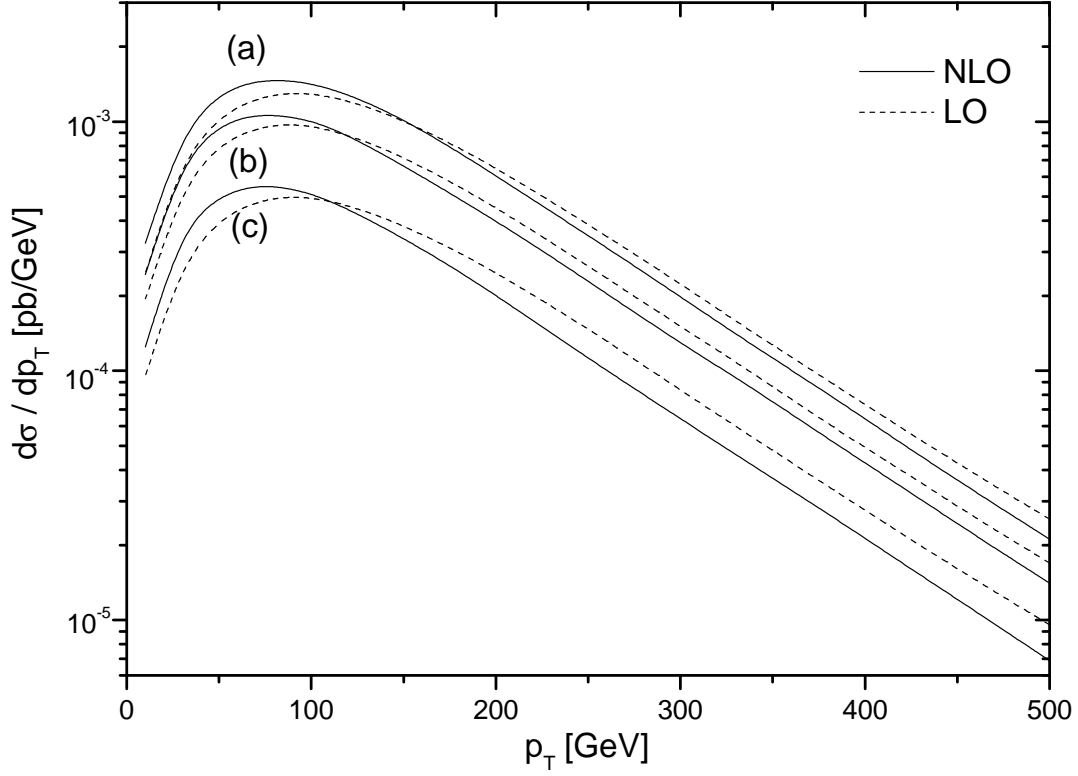


FIG. 13: Differential cross sections in the transverse momentum p_T of $\tilde{\chi}_1^-$ for the $\tilde{t}_1\tilde{\chi}_1^-$ production at the LHC, assuming $\mu = -200$ GeV and $m_{\tilde{t}_1} = 250$ GeV. For (a), $\tan\beta = 30$ and $M_2 = 600$ GeV; for (b), $\tan\beta = 30$ and $M_2 = 300$ GeV; for (c), $\tan\beta = 4$ and $M_2 = 300$ GeV.